For Geofluids Special Issue

Geothermal Systems: Interdisciplinary Approaches for an Effective Exploration

Tectonic evolution of the Southern Negros Geothermal Field and implications for the development of fractured geothermal systems

Loraine R. Pastoriza[1,2], Robert E. Holdsworth[1], Kenneth J.W. McCaffrey[1], and Edward Dempsey[1,3]

[1]Department of Earth Sciences, University of Durham, Durham, DH1 3LE, United Kingdom

[2]Geosciences and Reservoir Engineering Group, Energy Development Corporation, Ortigas, Pasig City, 1605, Philippines

[3]Department of Environmental Sciences, University of Hull, Hull, HU6 7RX, United Kingdom

Correspondence should be addressed to Loraine R. Pastoriza; pastoriza.lr@energy.com.ph

Abstract

Fluid flow pathway characterisation is critical to geothermal exploration and exploitation. In fractured geothermal reservoirs, it requires a good understanding of the structural evolution together with the fracture distribution and fluid flow properties. A fieldwork-based approach has been used to evaluate the potential fracture permeability characteristics of a typical high-temperature geothermal reservoir in the Southern Negros Geothermal Field, Philippines. This is a liquid-dominated resource hosted in the andesitic Quaternary Cuernos de Negros Volcano, Negros Island. Fieldwork reveals two main fracture groups based on fault rock characteristics, alteration type, relative age of deformation, and associated thermal manifestation, with the youngest fractures mainly related to the development of the current geothermal system. Fault kinematics, cross-cutting relationships, and palaeostress analysis suggest at least two distinct deformation events under changing stress fields since probably the Pliocene. We propose that this deformation history was influenced by the development of the Cuernos de Negros Volcano and the northward propagation of a major neotectonic structure located to the northwest, the Yupisan Fault. A combined slip and dilation tendency analysis of the mapped faults indicates that NW-SE structures should be particularly promising drilling targets under the inferred current stress regime, consistent with drilling results. However, existing boreholes also suggest that NE-SW structures can act as effective channels for geothermal fluids. Our observations suggest that these features were initiated as the dominant features in the older kinematic system and have then been reactivated at the present-day.

Introduction

Permeability, heat source, fluid recharge and capping mechanism are the vital elements to consider during the development of a geothermal reservoir [1, 2]. In a typical subduction-related geothermal system like those seen in the Philippines, the reservoir is mostly hosted in crystalline rocks in which permeability arises mainly from fractures, and less from the intrinsic permeability of the reservoir rocks [3]. It is therefore necessary to understand the type of fractures present, the fracture development history, and the nature of the transmissive present-day fracture networks developed at depth prior to tapping the reservoir through drilling. Ultimately such understanding should allow geothermal production to be maximised through targeting optimal fractures in the subsurface.

However, the structural modelling of sub-surface reservoirs in volcano-hosted geothermal systems has its own challenges. Sub-surface analyses using seismic refraction and reflection data are difficult to use as thick volcanic rocks are usually opaque to seismic waves and geological structures are often difficult, or impossible, to image [4]. Resistivity data is commonly used to visualise the reservoir structure based on the implied fluid content and development of alteration zones [5]. Although this can highlight the presence of large-scale structures, it is still challenging to identify reservoir-scale fracture networks using this technique. Additionally, at the early stages of geothermal exploration, carrying out geophysical surveys (e.g. gravity, resistivity, seismic), poses large financial risks to the developer. Thus, it is important to first maximise surface geological data before moving forward with the exploration stages. This work aims to illustrate how to better utilise surface geological data in understanding fractured geothermal systems using the Southern Negros Geothermal Field (SNGF) as a case study.

The SNGF lies in the municipality of Valencia in southwest Negros Oriental, Philippines. It is a volcano-hosted, high-temperature geothermal system, with temperatures ranging between 200 to 300°C, sitting on the northeastern flanks of the Cuernos de Negros (CDN) volcanic edifice (Figure 1). It is liquid-dominated with localised two-phase zones [6] containing fluids which are generally

neutral in pH, moderately saline, and have low gas content [7]. The field was commissioned in 1983 with a total installed capacity of 192.5 MWe. However, despite its long history of geothermal exploration and development, its fracture systems are still poorly understood.

Here, we use field and thin section observations to establish a deformation history for the SNGF particularly highlighting its role in influencing the development of the geothermal system. Given the limitations of outcrop quality and distribution that are typical in tropical countries (e.g. high rates of weathering and erosion and extensive vegetation cover) and the effects of volcanism (i.e. recent phreatic eruption of the volcanic centers may cover or erode exhumed structures), methodologies that optimise the field data are also examined. From the mapped structures, slip and dilation tendencies are evaluated and we show how these results could relate to and influence a drilling strategy for the SNGF.

Regional geological setting

The Philippine Archipelago is where four tectonic plates- SE Eurasia, Philippine Sea, Pacific, and Indo-Australia meet [8]. The largely aseismic Palawan-Mindoro microcontinent lies to the west representing a fragment rifted from mainland Eurasia in the mid Cenozoic, and to the east, lies the seismically active Philippine Mobile Belt on which the majority of the country is located (Figure 1a;). The latter region is an actively deforming zone composed of terranes of various affinity (i.e. from the ancient Philippine Sea Plate and the Indo-Australian margin) [9] that is bordered by subduction zones of opposing polarities: the west-dipping Philippine Trench and East Luzon Trough to the east; and the east-dipping Manila, Negros, Sulu, and Cotabato Trenches to the west (Figure 1a, [10-12]). Shallow earthquakes are dispersed across the Philippine Mobile Belt indicating its continued active deformation due to plate tectonic forces [8].

Traversing almost the entire length of the country, from northwest Luzon to southeast Mindanao, is the >1200km long sinistral Philippine Fault (Figure 1a) which has formed due to the oblique convergence of the Philippine Sea Plate with the Philippine Mobile Belt [14]. It is suggested that the

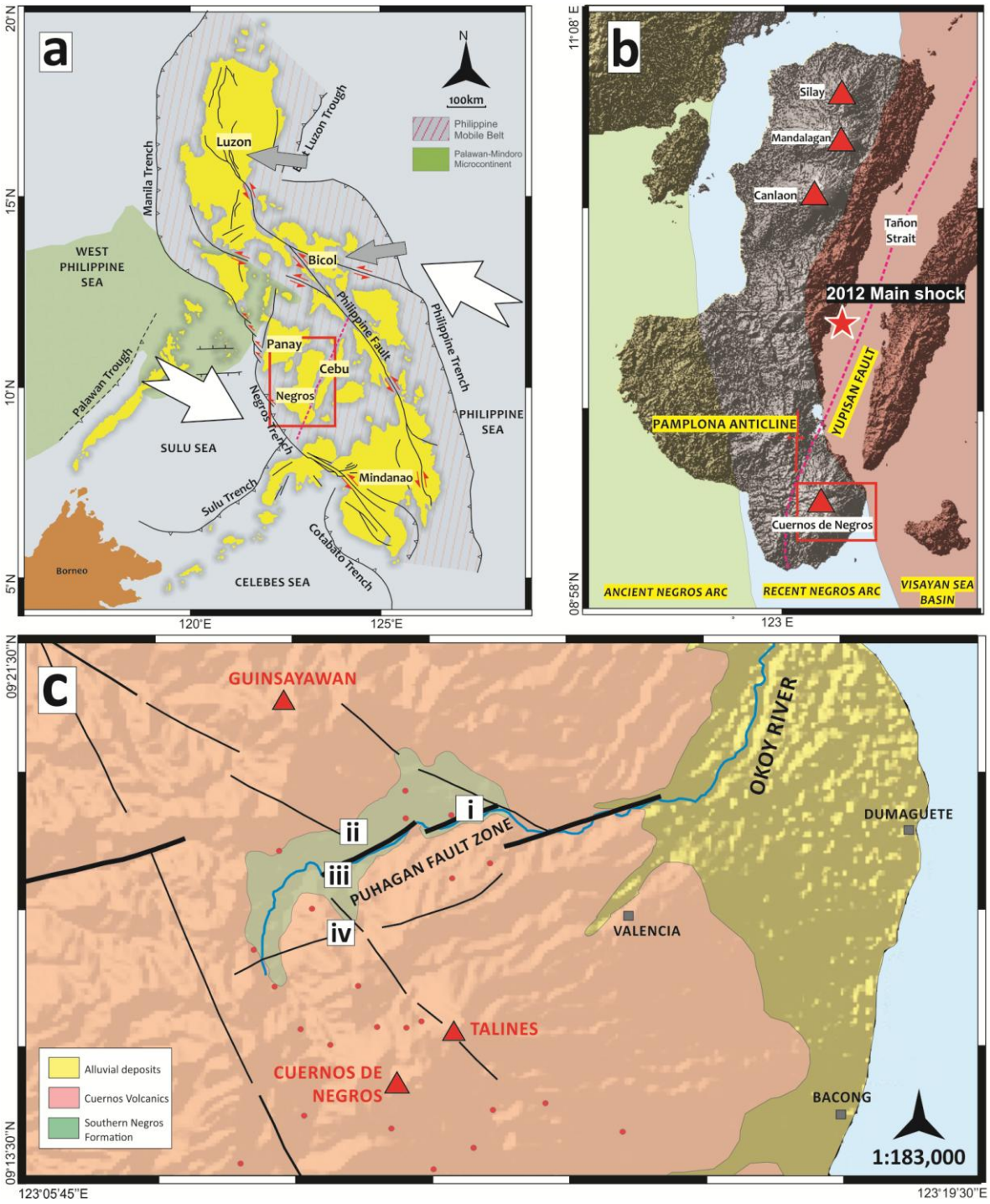

Figure 1. Regional tectonic setting and location of SNGF. (a) Major tectonic structures of the Philippines after Aurelio [13]. Large white arrows are plate motion directions [14, 15]. Grey arrows are the horizontal maximum compression orientations measured in Bicol in Lagmay *et al.* [16] and in Luzon in Yu *et al.* [17]. Red box represents the boundaries of the next figure. (b) Negros Island, showing the Negros volcanic arc in red triangles and the estimated trace of Yupisan Fault in dashed dark pink, overlain by the approximate boundaries of the tectono-stratigraphic terranes. Red box represents the boundaries of the figure below it. (c) Simplified map of SNGF encompassing the CDN volcanic complex showing the key lineaments identified in this study (black line), course of Okoy River (blue), volcanic edifices within the complex (red triangle), and estimated location of thermal manifestations (red dots), overlain by a simplified geological map of the field from Rae *et al.* [18] and PNOC-EDC internal reports. Boxes (i) to (iv) are the location of the outcrops discussed in this paper. (b) and (c) overlays 90m SRTM DEM data from Jarvis *et al.* [19].

Philippine Fault formed 4Mya after the plate convergence changed from north to NNW with respect to Eurasia, although its northern segment appears to have been initiated much earlier (10 Ma) [13]. GPS data show that the Philippine Fault has a slip rate of 2 to 3cm/yr [13, 20] or 2.4 to 4cm/yr [17] which represents a third of the oblique convergence of Philippine Sea Plate, while the two-thirds is accommodated along the Philippine Trench and other major structures across the country [13]. Maximum compression, σ_1, from recent studies is oriented between 90 to 110° in Luzon [17] and approximately east-northeast in Bicol region [16].

Geology of Negros

Negros Island is made up of three Cenozoic-Quaternary tectono-stratigraphic terranes that represent part of the subduction arc system related to the Negros Trench (Figure 1b) and are underlain by oceanic volcaniclastic basement, which is thought to be Cretaceous in age [11, 21]. From west to east in Negros, two overlapping volcanic arcs of different ages, the Ancient and Recent Negros Arcs, and the sedimentary Visayan Sea Basin are present (Figure 1b; [11, 22]).

The Ancient Negros Arc comprises Eocene to Oligocene andesitic to dacitic volcanic and clastic rocks intruded by a Miocene dacitic diatreme complex [22]. It is highly mineralised, hosting the Bulawan intermediate-sulphidation gold deposit, the gold-poor Sipalay deposit, and the Hinobaan porphyry copper and molybdenum deposits [22], all of which are situated in the southwestern part of Negros. The Recent Negros Arc [11] or Negros Belt [23] is composed of Middle Miocene to Pliocene andesite flow breccias, volcaniclastics and conglomerates that are overlain by Late Pliocene andesitic volcanics and Quaternary andesite and basalt stratovolcanoes [22]. Geomorphologically, the recent arc is represented by a 260 km chain of volcanoes, four of which are on Negros Island (from north to south): Mt. Silay, Mt. Mandalagan, Mt. Canlaon, and Cuernos de Negros (CDN) [23] (Figure 1b). Of these four, only Canlaon is active with the most recent volcanic activity (i.e. release of white plumes and volcanic earthquakes) occurring in January 2018 [24], whilst Mandalagan and Cuernos de Negros are considered to be in their fumarolic stage [23].

Towards the east, the Visayan Sea Basin, representing the back-arc region of the Negros arc system [25] underlies the eastern coast of Negros, the Tañon Strait, and the islands of Cebu and Bohol (Figure 1b). The basin is filled with up to 4 km thick carbonate and volcaniclastic sequences deposited from the Middle Oligocene to Middle Miocene [11]. These are generally folded, with fold axes oriented NNE-SSW on the average. Rangin *et al.* [25] proposed that the Visayan Basin comprises a series of NNE-SSW-trending horst and graben structures, with the Tañon Strait corresponding to a graben, which cuts the earlier folds. However, recent studies by Aurelio *et al.* [26] following the Mw 6.7 earthquake in February 2012 propose the existence of a northeast-striking and northwest-dipping reverse fault, the Negros Oriental Thrust, that runs from west of CDN towards eastern offshore Negros.

Southern Negros is formed mainly by Quaternary volcanic rocks that are part of the Recent Negros Arc. Miocene to Early Pleistocene clastics have been locally exposed in the northwest of CDN as part of the Pamplona Anticline - a result of the regional fault-propagation folding associated with the Negros Oriental Thrust, which is mapped onshore as the Yupisan Fault (Figure 1b; [26, 27]).

Local geology

Deep drilling to 3300 m depth over the last three decades reveals that the CDN volcanic complex was created by several volcanic and intrusive events ([26]; Figure 2). The oldest rocks drilled are thick, 990 m on average, Miocene volcanic sequences of altered andesites intercalated with tuffs and calcarenites with occasional volcanic and sedimentary breccias, known as the Puhagan Volcaniclastic Formation. These rocks are cross cut by the Nasuji quartz monzodiorite to micromonzodiorite pluton which led to the formation of a metamorphic aureole known as the Contact Metamorphic Zone. Geochronological studies of the pluton have yielded contradicting age of Miocene (10.5 Mya using K-Ar in [28] [29]) and Pleistocene (0.7 to 0.3 Mya using Ar-Ar in Rae *et al.* [18]). By the Early Pliocene, the Okoy Sedimentary Formation and overlying undifferentiated andesitic volcanics and pyroclastics of the Southern Negros Formation were deposited. All the

above mentioned formations have been intruded by at least two dyke events during the Pliocene. Lateral and vertical variations of lithologies and facies within the Okoy Sedimentary and Southern Negros Formations have been detected during drilling of wells and indicate the presence of a palaeo-topography within the SNGF in which the western sectors were uplifted in the Early Pliocene [28]. This is confirmed by fossil assemblages within the two formations in the western region which are characteristic of a shallow to sub-aerial environment, whilst those preserved in the eastern region are typical of a deep marine environment [28]. These rocks are overlain by the Quaternary-aged andesitic Cuernos Volcanics, which can be subdivided into different members depending on which volcanic edifice of the CDN volcanic complex they are associated with (i.e. main CDN peak, Talines, Guinsayawan, Figure 1c). Radiocarbon dating of charred wood within the Cuernos Volcanics suggests a youngest eruption age of 14,450 years [29]. These young volcanics cover much of the surface of the present-day CDN volcanic complex, with exposures of the older Southern Negros Formation limited to the downstream river valley area of the E-W Okoy River (Figure 1c).

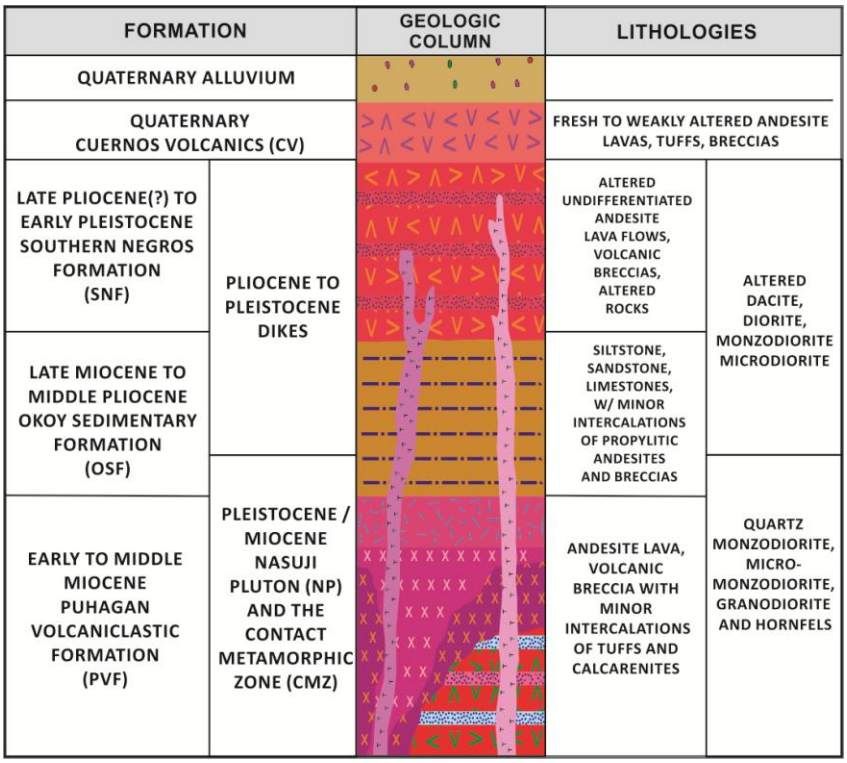

Figure 2. Geological column of the CDN volcano as encountered in the boreholes. Corresponding ages are in the first column, whilst their general lithologies are in the third column. Note that although there is a strong geochronological evidence that the Nasuji Pluton is younger, there is no clear evidence of its intrusion into the younger lithologies

157 Topographic lineament analysis using combined high and low resolution digital elevation models
158 carried out indicates a dominance of ENE-WSW and NW-SE to NNW-SSE features (Figure 1c). The
159 most conspicuous lineaments are the ENE-WSW-trending set that coincide with the Okoy River, and
160 appear to be discontinuous and arranged as right-stepping *en echelon* features, representing the
161 traces of a known fault network in SNGF, designated here as the Puhagan Fault Zone (Figure 1c).
162 Geomorphological kinematic indicators such as push-up ridges observed along the trace of this fault
163 zone suggest it has a dextral sense of movement.

164 ## Mapped structures

165 The SNGF rocks exposed at the surface are exclusively deformed by brittle structures, including
166 different types of fractures, such as faults, joints, and veins. The fractures observed in 84 out of the
167 135 outcrops that were studied can be sorted into two main groups, here termed Group 1 and
168 Group 2. This two-fold classification is mainly based on the types of associated fault rocks, key
169 alteration minerals, and the host rock which the fractures cut. The field characteristics are
170 summarised in Table 1 and discussed in detail in the sections that follow.

171 **Table 1. Summary of field characteristics of the two fracture groups mapped in SNGF.**

	Group 1	Group 2
Fault rocks	Cohesive and cemented (cataclastic)	Generally non-cohesive/poorly cemented Open fractures in some
Key alteration minerals	Abundant pyrite Amorphous silica Quartz rare Cu-sulfides	Abundant clays Quartz Native sulphur Zeolites, calcites, gypsum
Kinematics	Mostly E-W (+/-) sinistral	Mostly NW-SE oblique dextral
Host rocks	Older Southern Negros Fm. Host has been completely altered previously	All lithologies Both altered and fresh rocks
Alteration pattern	Restricted to fractures	Diffuse or restricted to fractures
Other key observations		Usually related to recent (active/inactive) thermal activity

Group 1 fractures

Group 1 structures are restricted to the river exposures along the ENE-draining Okoy River gorge and one of its SE-draining tributaries (Figure 1c.i and 3). This restricted region corresponds to the exposures of the Southern Negros Formation adjacent to the river, but it is most likely that these structures may be widely developed in the older rock strata that underlie much, if not all, of the Quaternary CDN edifice. Textures in the Southern Negros Formation in general are almost completely obliterated due to the effects of hydrothermal and supergene alteration, appearing as dark grey with yellowish to reddish patches due to iron oxide and sulphur deposition. Ghost phenocrysts are observed suggesting that the protoliths were porphryitic, but the crystals have been almost entirely replaced by clays.

Group 1 structures form as conspicuously grey fractures filled with abundant <1 mm to 2 mm grainsize pyrite crystals (Figure 3). Along the central part of the Okoy River gorge, these are E-W to WNW-ESE-striking (096°/62°-S) sinistral faults with slickenlines typically pitching <15°, and run sub-parallel to the trace of the main Puhagan Fault Zone. A fault core is recognised and is interpreted to correspond to the region where most shear displacement has been localised. A series of cm- to m-spaced ENE-WSW-trending sub-vertical faults here are filled with cataclasite comprising fine angular (rare 10 mm, mostly <5 mm grainsize) fragments of altered protolith, weakly foliated in some cases, set in a cemented dark grey matrix (almost clay-sized, <1 μm) (Figure 3a). Petrographic work on the fault rock samples suggests a dominance of pyrite mineralization within a generally cryptocrystalline matrix carrying identifiable fine crystals of pyrite, quartz, opaque minerals, and amorphous silica (Figure 4a). Sinistral senses of motion are indicated by microscopic kinematic indicators (i.e. *en echelon* features) (Figure 4a). Few offset markers are seen along the fault plane, so it is difficult to estimate total fault displacements.

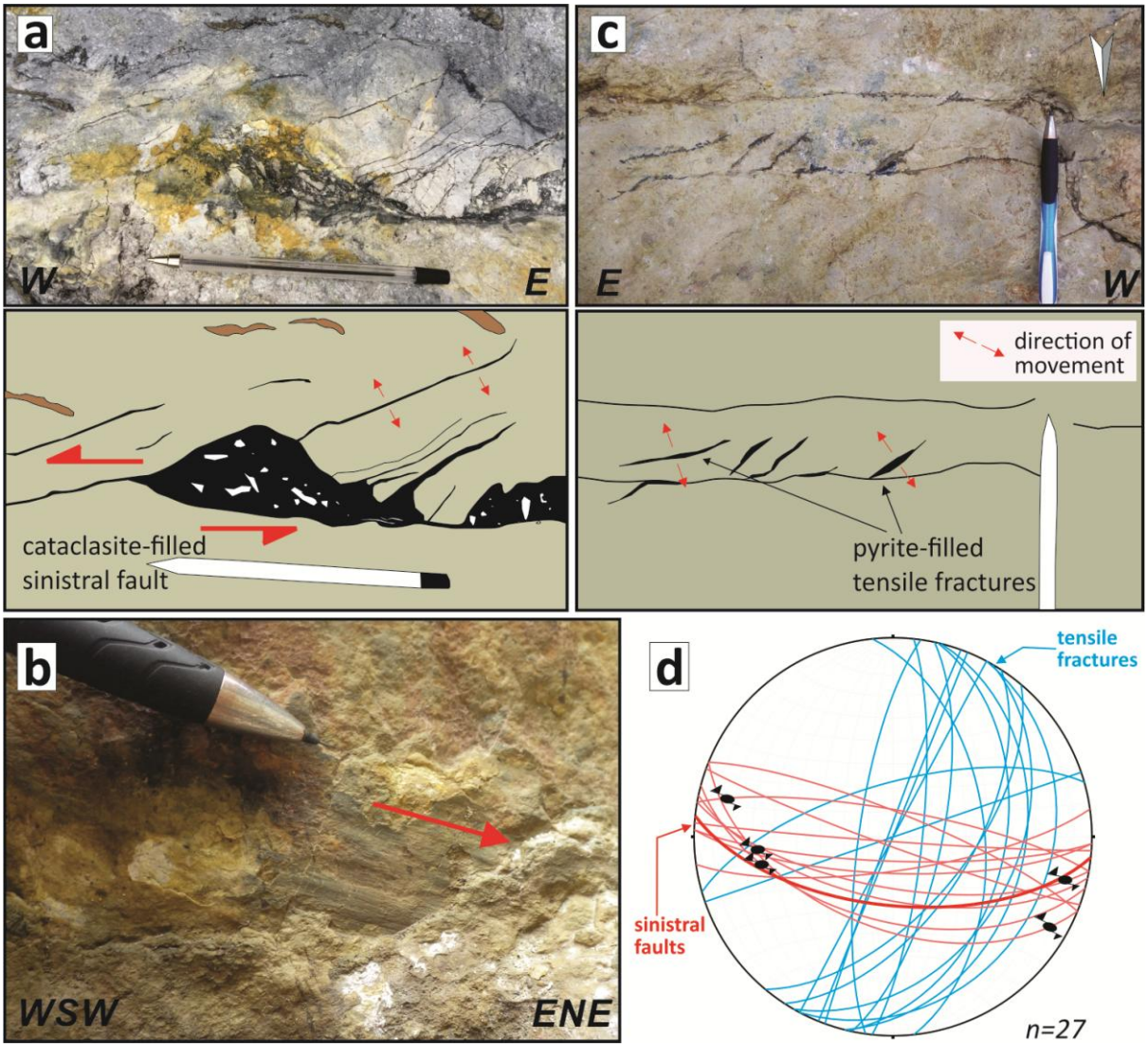

Figure 3. Group 1 fractures at the macroscale. (a) Close-up photo of the E-W to WNW-ESE sinistral faults showing the cataclastic core mapped along Okoy River (refer to Figure 1c.i for the location). (b) Slickenline preserved on the sinistral fault. (c) Pyrite-filled veins (located at Figure 1c.i and ii). (d) Fault planes (red) and tensile fractures (blue) represented in an equal area lower hemisphere stereonet.

The sinistral faults along the downstream of Okoy River are associated with smaller NE-SW to E-W-striking sinistral fractures based on millimeter-scale offsets, interpreted to be synthetic Riedel shears that are completely cemented and mineralised. Likewise, dense arrays of NE-SW-striking steeply dipping quartz- and pyrite-filled tensile fractures are observed (in i and ii in Figure 1c). Fine (~1 to 2 µm) gypsum crystals also occur within some mineral fills. The tensile fractures lie obliquely anticlockwise to the main sinistral faults or form as *en echelon* features (Figure 3c). Where the two key alteration minerals, pyrite and quartz, are present, they usually occur as anhedral crystals, but

when pyrite occurs on its own, it is typically sub- to euhedral, with crystals that can be as large as 5 mm and usually oriented perpendicular to the fracture walls. Cockade overgrowth textures [30] within some of the euhedral pyrite crystals are also observed in thin section (Figure 4b).

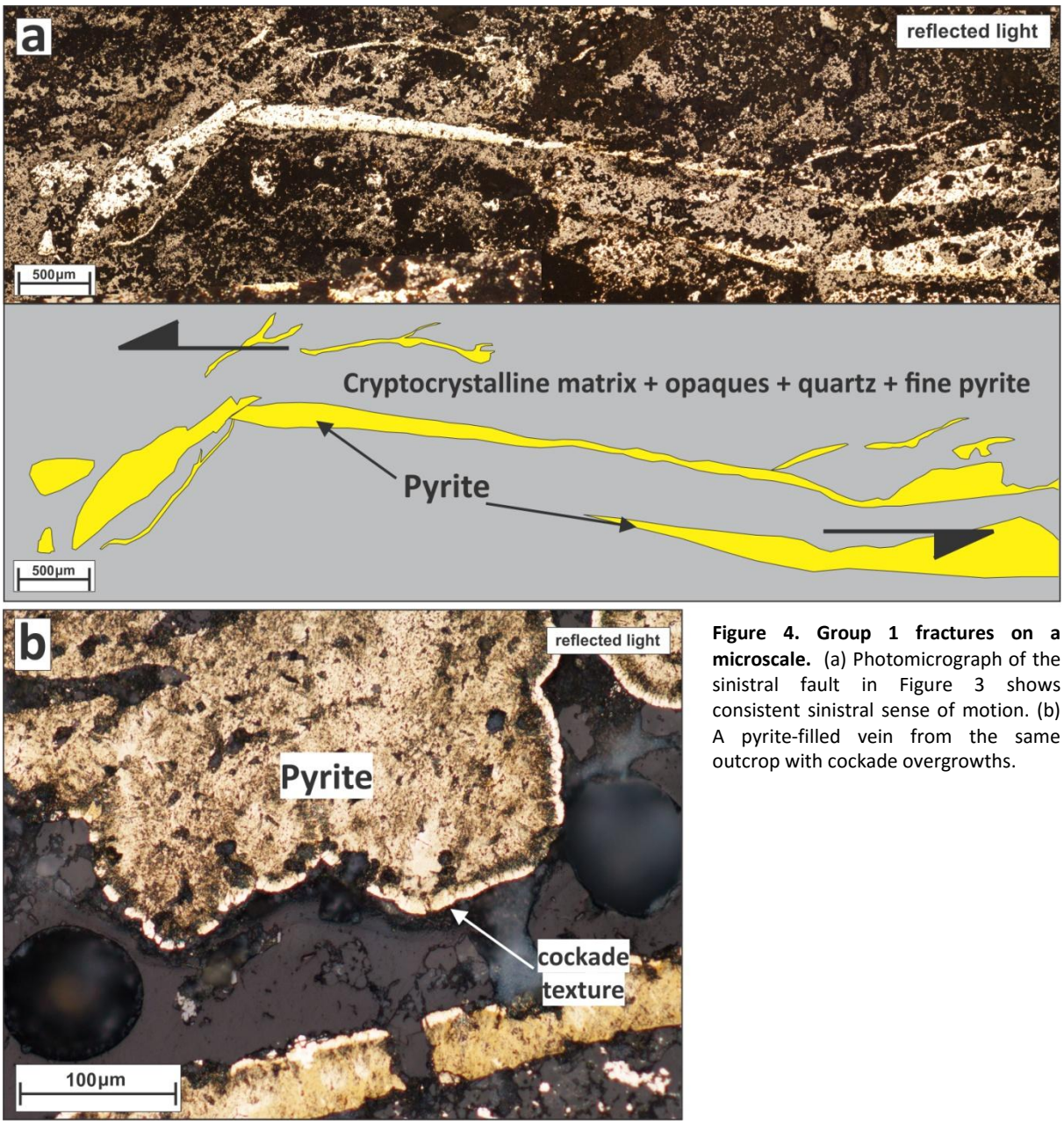

Figure 4. Group 1 fractures on a microscale. (a) Photomicrograph of the sinistral fault in Figure 3 shows consistent sinistral sense of motion. (b) A pyrite-filled vein from the same outcrop with cockade overgrowths.

Group 2 fractures

Group 2 fractures are the dominant and ubiquitous features throughout the SNGF. Of the 84 outcrops mapped within the geothermal reservation, 90% expose faults classified under this group. The majority of large fractures are generally oriented WNW-ESE to NNW-SSE, usually steep to

moderately dipping, exhibiting either normal, dextral, or normal-dextral oblique senses of movement, where kinematic indicators are preserved (Figure 8). Smaller, but poorly preserved and less frequent NE-SW and NNE-SSW-trending fractures have also been mapped. Where shear sense can be determined, it is often observed in normal faults, and more rarely, in sinistral structures.

Group 2 fractures generally contain incohesive fault rocks, typically fault gouges and fault breccias (Table 1). Occasionally, sharp slip planes or localised brittle shear zones occur. These structures cut both completely altered and fresh volcanic rocks. In some outcrops, the damage zones belonging to faults at least ten meters long have widths ranging a few centimeters to tens of meters. Most outcrops, however, preserve evidence that the brittle deformation is followed by intense clay alteration localised along the fault zone. Active and recently active thermal manifestations - such as hot springs, gas seepages, or hot ground - are often found along or adjacent to the traces of these Group 2 fractures, implying the permeability present on these sets of structures that channel hydrothermal fluids. This further suggests that these faults play critical roles in the geothermal development and present-day fluid flow.

Two outcrops at localities 81 and 104 feature some of the best preserved Group 2 structures and are discussed in detail below (more outcrop discussion can be found in Pastoriza [27]. These faults show the typical characteristics of the group, particularly, the dominant NW-SE fractures. In locality 81, this fault is a large dextral-oblique structure, whilst at locality 104, the fault has a dip-slip normal sense of movement.

Locality 81

This WNW-ESE-oriented dextral-oblique fault (mean orientation of 118°/80°-S) cuts moderately to intensely altered porphyritic andesite (Fault A in Figure 5, refer to box iv in Figure 1c for the location). Narrow 40 to 60 cm wide fault cores, with wider 150 cm intensely damaged zone, are flanked by a still broader 600 cm wide moderately damaged zone. Background fracturing is present outside the damaged zones on both sides of the fault zone (Figure 5b). The fault preserves a crudely

241 banded, variably altered pale gouge, formed by moderately to completely pulverised host rocks. In
242 most parts, the fault is clay-altered and lined with fine-grained, hematite-filled and coarse-grained
243 fibrous gypsum veinlets. Some less altered clasts of the porphyritic andesite protolith up to 15 cm in
244 diameter are preserved within the fault core. Fault kinematics are gleaned from slickenlines and
245 slickenfibres, varying between a purely dextral to less common dip-slip normal sense of motion
246 (Figure 5d). Offset markers are poorly preserved, but are most likely minimal, suggesting generally
247 small finite strains. One to two centimeter thick gypsum veins have crystallised along the walls of the
248 fault planes and are oriented oblique to the wall (Figure 5d) suggesting that crystallization is
249 contemporaneous with fault movements. Generally NW-SE-trending unfilled tensile fractures are
250 observed to have formed adjacent to the fault plane, which are kinematically consistent with the
251 main dextral shear sense inferred for the faults.

252 A left-stepping, generally E-W-striking dextral-normal fault occurs immediately to the south of the
253 dextral fault (Fault B in Figure 5). A 25 to 50 cm fault core here is filled with intensely oxidised fault
254 rock (Figure 5e). Gypsum precipitation is preserved around some of the sheared margins of trapped
255 protolith fragments. At the southern end of the outcrop, a network of associated smaller normal
256 faults are generally oriented ENE-WSE to WNW-ESE with discrete slip planes (Figure 5a/b). Fault
257 cores are not as well developed here compared to the two structures described above, but there is a
258 strong indication that they channel hydrothermal fluids based on the formation of diffuse alteration
259 haloes around most fractures. The network of smaller normal faults also appears to connect with
260 the larger ones. Where they join, evidence of enhanced permeability is noted, such as the presence
261 of empty vugs and suspected recent open fractures marking the sites of recently inactive gas
262 seepage fissures, and preservation of increased deposition of secondary minerals (e.g. gypsum,
263 travertine; Figure e.ii).

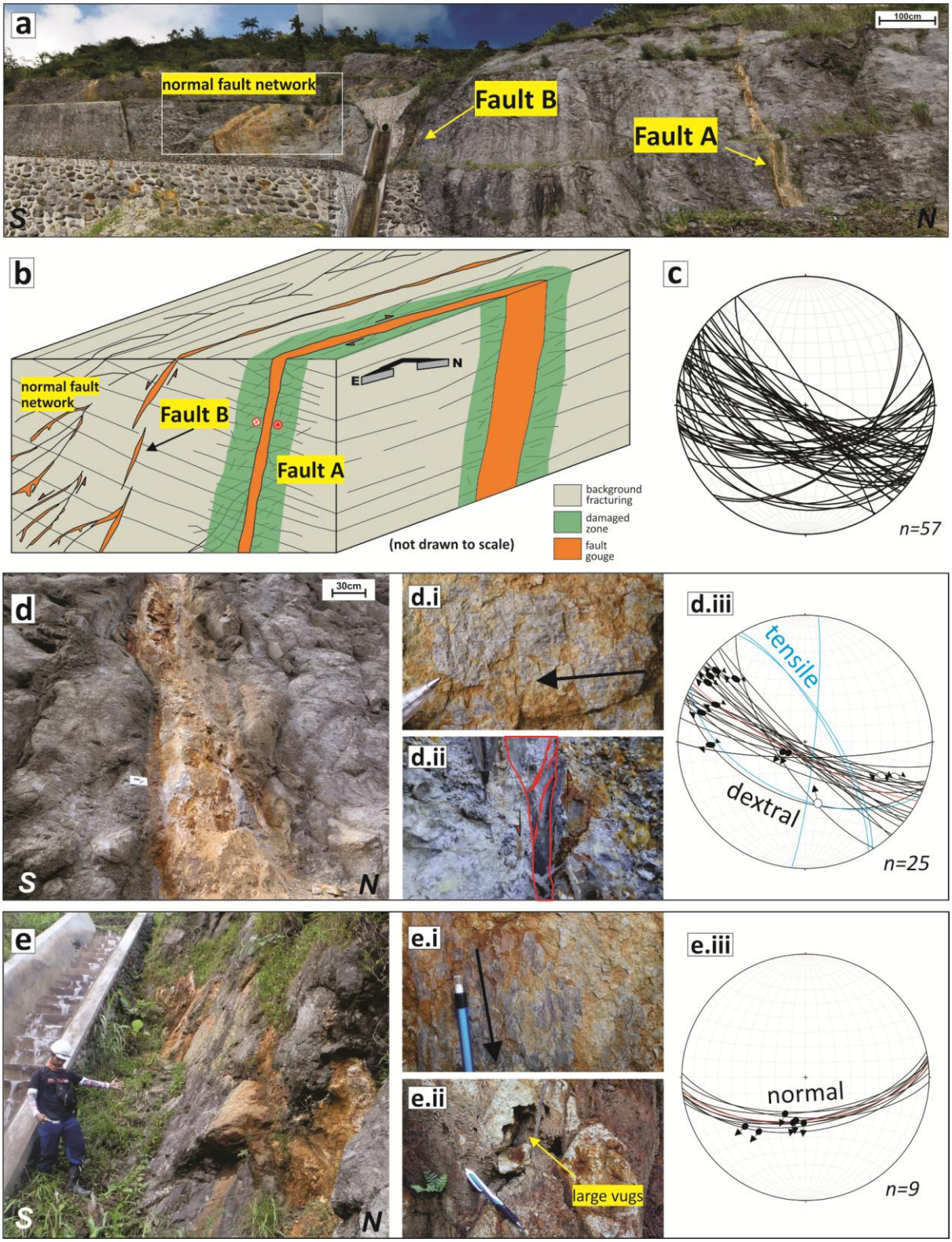

Figure 5. Group 2 NW-SE dextral and normal faults. (a) Panorama of the entire outcrop (refer to Figure 1c.iv for the location). (b) 3D sketch of the faults showing the location of the two large faults discussed in-text, and their sub-parallelism and potential linkage by an array of smaller normal faults. (c) Stereographic projection of all the fractures mapped in the locality. (d) The main dextral fault, Fault A, showing the horizontal slickenlines (i), oblique gypsum crystals (ii), and the stereoplot (iii) which has tensile fractures in blue and average orientation of the fault plane in red. (e) The large normal fault, Fault B, and its subvertical slickenlines (i), portions of suspected enhanced permeability (ii), and stereoplot (iii).

Locality 104

A NW-SE trending moderately north-dipping fault (131°/58°-N on average) runs perpendicular to the Okoy River (Figure 6; located at box iii in Figure 1c). It cuts an intensely silicified andesite outcrop that can be traced through both sides of the ravine, forming cave-like features on either side (Figure 6a). Preserved slickenlines and steps in the hanging wall suggest dip-slip normal senses of shear. The magnitude of displacement is difficult to assess due to the limits of exposure and lack of discernible offset markers in the wall rocks. The hanging wall is clearly exposed whilst the footwall is less distinct (Figure 6b). The fault core for this structure is a 12 to 15 cm thick gouge in which several fractured lensoid slivers of the host rock are entrained. The gouge-filled fault core is only exposed by hammering, and has a thin film of what appears to be amorphous silica on its surface. Thin section studies indicate intense silica-replacement and fracture infill of both the host rock and the fault rock (Figure 6e). Smaller fractures within the fault zone are oriented mostly WNW-ESE and are interpreted to be conjugate fractures to the main normal faults (Figure 6d). Where these smaller fractures join, local pull-apart structures or dilational jogs are observed (Figure 6c). In many cases, uncharacterised fine white crystals have precipitated around these structures which strongly suggest a recent outflow of mineral-rich fluids and/or gas. NNW-SSE sealed quartz veins and NW-SE unfilled tensile fractures are observed throughout the exposure which is consistent with the inferred direction of extension for this normal fault (Figure 6d).

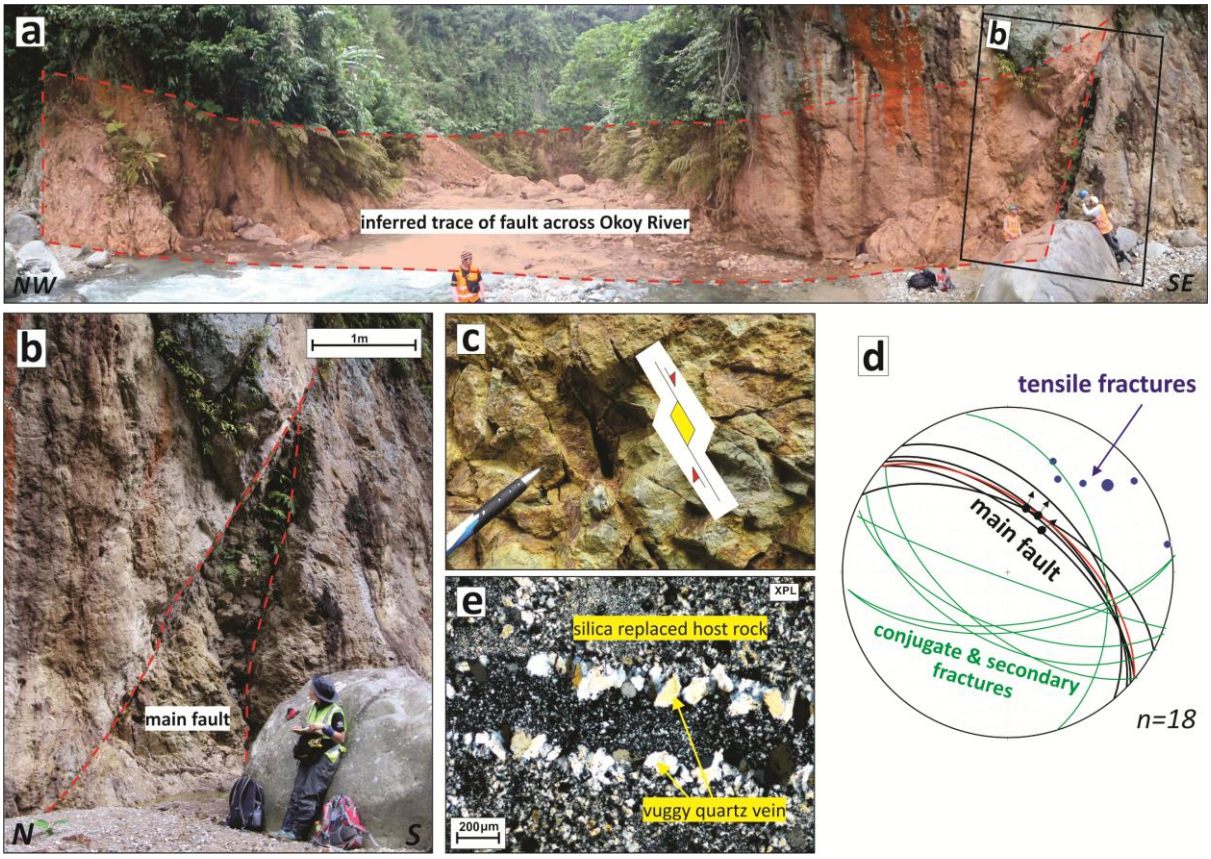

Figure 6. Group 2 NW-SE normal fault. (a) The structure at the midstream of Okoy River with the estimated fault trace projected as a red plane (see to Figure 1c.iii for the location). (b) Section view of the SE side of the ravine showing the main structure. (c) Close-up photo of the small-scale dilational jogs which are common in the damage zone. (d) Stereonet showing the main fault planes in black, the average plane in red, secondary and likely conjugate structures in green. Poles to the tensile fractures and veins are represented as blue dots. (e) Photomicrograph of the host rock, completely replaced by silica, and also, cut by a quartz vein.

Cross-cutting relationships

Group 1 structures are limited to the older Late Pliocene to Pleistocene Southern Negros Formation and are not observed in the younger lava flows and pyroclastics belonging to the Quaternary Cuernos Volcanics. Group 2 structures, on the other hand, are observed in both lithological formations. Given the older age of the lithological formation where Group 1 fractures are found, this suggests that they are most likely to have formed earlier than Group 2 and prior to the deposition of the Quaternary and Recent rocks (i.e. Cuernos Volcanics). The distinct characteristics of the associated fault rocks from the Group 1 and Group 2 fractures (Table 1) also suggests that the two groups of fractures have formed under different deformational conditions at different times.

Cross-cutting relationships observed in the field support the relative age hypothesis. In the downstream regions of the Okoy River valley, sinistral NE-SW-trending fractures interpreted as

Group 2 faults based on the development of millimeter-scale gouges with sulphur and oxides formed along exposed surfaces, everywhere offset Group 1 WNW-ESE sinistral pyrite-filled fractures by up to 4 cm (Figure 7a). Offsetting relationships are also observed for two sets of tensile fractures trending ENE-WSW and NNW-SSE, interpreted to belonging to Group 1 and Group 2, respectively. Here, the NNW-SSE fractures cut through the ENE-WSW ones (Figure 7b), suggesting that Group 1 structures are older than Group 2.

Quartz- and occasionally sulphur-filled Group 2 fractures offset the pyrite-dominated tensile fractures of Group 1 (Figures 7c/d). In some cases, Group 1 tensile fractures here have reopened, either as pure Mode-I or as hybrid fractures (Figure 7c). Based on this evidence, the fracturing event that formed the Group 1 fractures is referred to as *Stage 1*.

There is also some field evidence that the Group 2 fractures may have accommodated more than one phase of deformation. This is based on several instances of Group 2 fractures being offset by other Group 2 faults with a different sense of slip which are inferred to have been reactivated. For example, in the northeast area of SNGF, a NW-SE-trending, gently dipping sinistral-reverse Group 2 structure offsets a steeply dipping Group 2 fault of similar trend by approximately one meter. An ENE-WSW- to E-W-trending Group 2 fault in the northern area of SNGF preserves both near vertical (pitch 84°) and sub-horizontal (pitch 20°) slickenlines (Figure 7e/g). These are related to normal and dextral senses of motion, respectively, based on slickenline stepping relationships. The steep lineations overprint the sub-horizontal slickenlines suggesting that the fault initiated as a dextral structure and was then reactivated with a dip-slip sense of motion.

More generally, a distinct group of NW-SE-oriented dip-slip faults are seen to consistently offset all other fractures. In many cases, these structures show evidence of overprinting slickenlines and in all cases, they reactivate as dip-slip structures rather than strike-slip features. It is therefore proposed that the Group 2 fractures, identified on textural and alteration assemblage grounds, show evidence for at least two deformation events, herein termed as *Stage 2a* and *Stage 2b.*

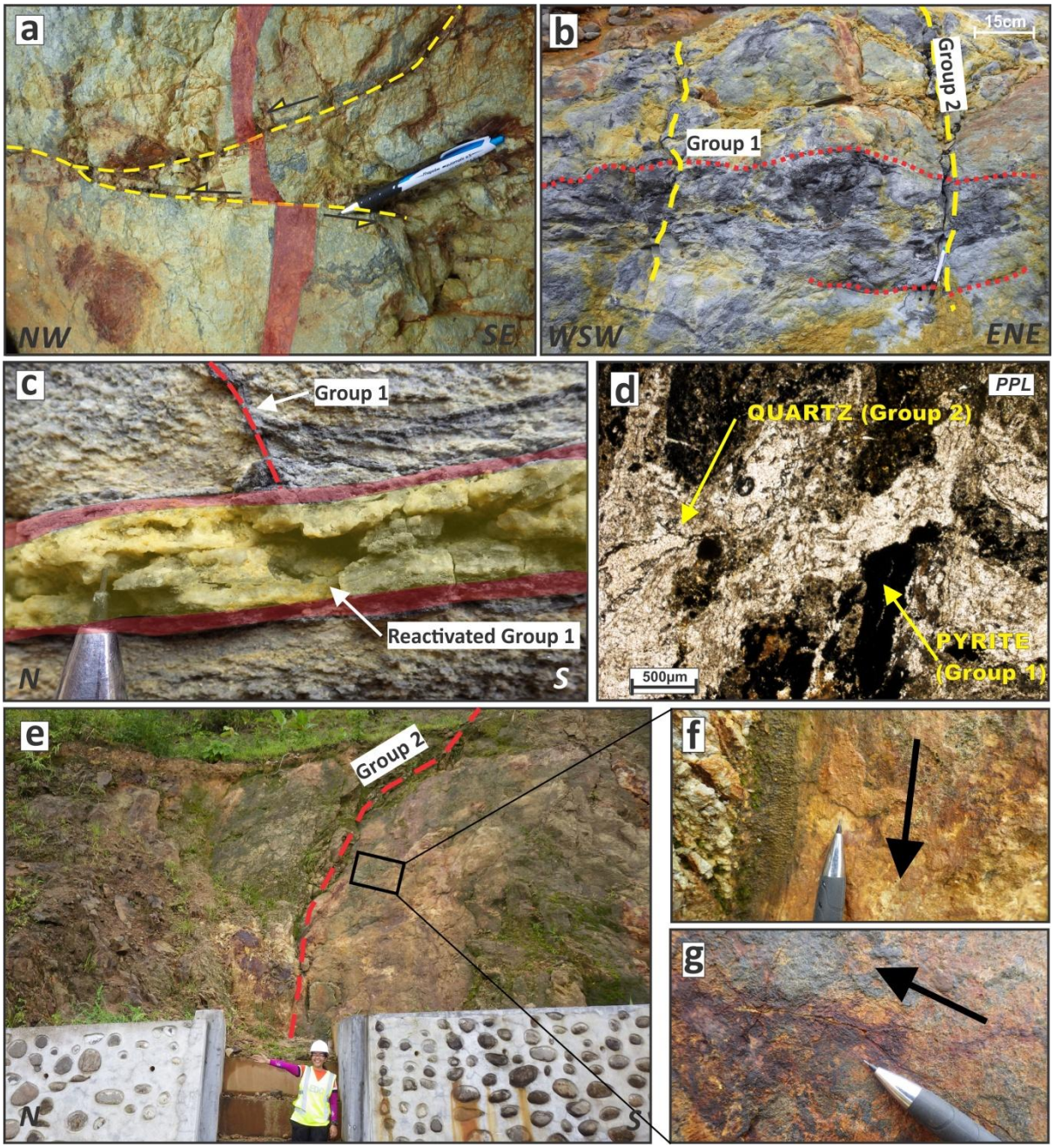

Figure 7. Cross-cutting observations. (a) NE-SW sinistral Group 2 fault (in yellow broken line) offsets a WNW-ESE sinistral Group 1 fault zone (in red). (b) Group 2 tensile fractures (yellow broken lines) also cut Group 1 tensile fractures (red broken lines). (c) Group 1 pyrite-filled (in red) tensile fracture is reactivated and filled with quartz with sulphur precipitates (in yellow). (d) Cross-cutting pyrite (Group 1) and quartz vein (Group 2) in thin section. (e) An E-W moderately-dipping Group 2 fault (red line) has preserved two sets of overlapping slickenlines – (f) near vertical and (g) sub-horizontal, suggesting two directions of movement along one fault.

Figure 8 summarises the key kinematic features of faulting during each of the stages. Stage 1 includes all the Group 1-classified fractures, which are mostly E-W-trending sinistral faults and NE-SW-oriented (rare NW-SE) tensile fractures. Approximately 70% of the Group 2 fractures are interpreted to have formed during Stage 2a. This is dominated by NW-SE-oriented normal and

dextral faults and NW-SE tensile fractures, and some N-S-striking normal and tensile fractures (Figure 8). Lastly, some NW-SE and E-W faults show evidence of later dip-slip normal movements and are considered to have formed during Stage 2b.

Palaeostress analysis

Following the classification of the mapped fractures into two stages based on field and microscopic characteristics, a stress inversion analysis was conducted to evaluate the possible stress conditions at the time of their formation. The inversion relies on the assumption that the faults and the blocks of rock they bound have not rotated significantly since their formation. This is a reasonably safe assumption given that the observed and inferred displacements of the key SNGF faults are minimal, suggesting that finite strains are overall low. The stress inversion was carried out in the Windows-based application, MyFault version 1.05, using the Minimised Shear Stress Variation inversion method which assumes that the magnitude of the shear stress on the fault is similar for all the fault planes at the time of rupture [31-33] (see Appendix 1 for details of the methods). Amongst the various methods of stress inversions considered, this yielded the minimum misfit angles (Appendix 1), and thus is considered to be the most appropriate for the SNGF dataset. A weighting scheme was further applied in the inversion based on the thickness and length of the mapped faults to give more significance to larger structures over smaller ones.

For Stage 1, σ_2 is calculated to be steeply plunging (66°/138°), whilst both σ_1 and σ_3 are horizontal to shallowly plunging, trending ENE and NNW-SSE, respectively (Table 2 and Figure 8). The calculated extensional direction, σ_3 is consistent with the poles to the majority of associated tensile fracture planes (Figure 8). With a shape factor of 0.31, the stress configuration suggests a strike-slip to transpressional tectonic setting.

During Stage 2a, the implied tectonic setting has changed to a strongly extensional or normal-faulting regime. The calculated σ_1 is vertical whilst the principal extension direction, σ_3, is E-W, which coincides with the poles to the mapped N-S tensile fracture planes (Figure 8).

Table 2. Palaeostress inversion results of all the fracture sets by fracturing events. Data were weighted based on the thickness of the deformation zone alone or together with the length of the lineament to minimise biases due to poor field exposures.

Stage	Weighting parameter	Number of data	Trend (plunge) of the principal axes, degree			Shape factor, δ	Mean slip misfit angle, deg
			σ_1	σ_2	σ_3		
Stage 1	N/A	5	243 (6)	138 (66)	336 (23)	0.31	18
Stage 2a	thickness	57	314 (82)	185 (5)	95 (6)	0.44	28
Stage 2a	thickness & length	57	269 (87)	1 (0)	91 (3)	0.48	37
Stage 2b	thickness	11	269 (55)	153 (17)	53 (29)	0.71	24
Stage 2b	thickness & length	11	275 (54)	155 (20)	54 (29)	0.72	23

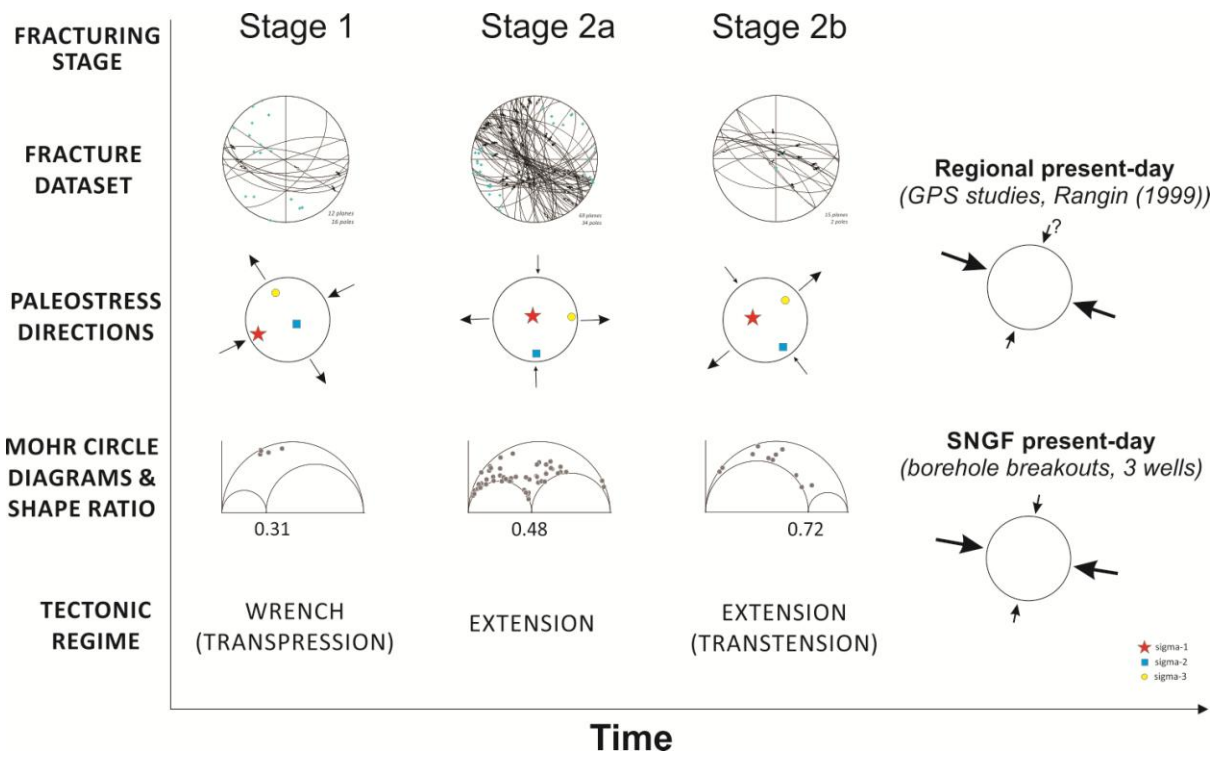

Figure 8. Summary of the palaeostress analysis results calculated per stage. Top row shows the stereographic projections of faults per stage with their corresponding slickenlines. Hollow symbols indicate a component of reverse sense of motion. Cyan stars represent poles of the tensile fractures. The Stage 2a and Stage 2b results are from the data which have been weighted by both the fault thickness and length. The smaller compression arrows in Stage 2a and 2b suggest that the event is mainly extensional, and thus, the magnitude of compression may be minimal. The question mark in the regional present-day direction indicates that only the maximum compression direction is given in the cited study. The smaller arrows are thus assumed.

384 During Stage 2b, σ_1 remained steeply plunging (55°/269°, Table 2) during a generally extensional or
385 transtensional tectonic regime with a shape ratio of 0.71. The S_{Hmax} is now oriented NW-SE.

386 The orientations of the principal stresses in Stage 2b appear to be similar to the present-day
387 configuration but with a swapped σ_1 and σ_2. The World Stress Map [15] reports, based on limited
388 data for Negros, a modern WNW-ESE and less common ENE-WSW-oriented S_{Hmax} in the southwest of
389 Negros and Tañon Strait. The focal mechanism of the 2012 earthquake generator as discussed in
390 Aurelio *et al.* [26] suggests that the $S_{Hmax} = \sigma_1$ is oriented NW-SE. GPS studies by Rangin *et al.* [34]
391 likewise suggest a NW-oriented (315°) convergence direction, similar in direction to that reported by
392 Kreemer *et al.* [35], which is parallel to the overall convergence direction estimated for the
393 Philippine Sea Plate [14]. Finally, restricted borehole breakout data from SNGF wells indicate that
394 S_{Hmax} is WNW-ESE. Overall, these present-day data suggest that the S_{Hmax} is generally oriented NW-
395 SE to WNW-ESE, consistent with the principal stress orientations determined for Stage 2b, except
396 that $S_{Hmax} = \sigma_2$. Thus, the youngest fractures in SNGF have probably formed in a stress field where
397 the principal stress axis orientations were similar to the present-day, but σ_1 and σ_2 may have
398 switched due to the perturbing effect of the volcanic edifice in the region of the SNGF as discussed
399 below.

400 **Slip and dilation tendency analysis**

401 An attempt to identify which of the mapped structures might be the most favorable drilling targets is
402 now presented, using a slip and dilation tendency analysis. The rationale here is that when a
403 structure has a higher tendency to slip under the present-day stress conditions, there is a greater
404 chance of increased fracture density and enhanced permeability [36]. Higher capacity to transport
405 fluids is also probable when a structure is more prone to dilate, since fault aperture is most likely to
406 readily enlarge. These concepts have been effectively applied, for example, in assessing fault
407 reactivation potential in deep enhanced geothermal systems in Germany [37] and in understanding
408 anisotropic transmissivity of the groundwater in the Yucca Mountain in Nevada [36].

All the analyses were carried out using 3DStress® version 5 software developed by the Southwest Research Institute. Present-day principal stress directions applied were based on the regional GPS studies of Negros Island (i.e. [34] and [38]). Stress magnitudes were estimated from the lithological overburden pressure (for the vertical stress, S_v), borehole leak off tests (for the minimum horizontal stress, S_{Hmin}), and the derived shape ratios from the palaeostress analysis (which allows calculation of the maximum horizontal stress, S_{Hmax}).

Overall, slip tendency values are quite low (<0.20) suggesting that in general, the structures in the SNGF are not prone to slip under the proposed present-day stress conditions. This contrasts with the strongly dilational tendency with widespread values approaching 1.0. The mapped steeply dipping to vertical NW-SE faults have the highest slip and dilation tendency followed by moderately dipping structures of similar orientations. The most stable faults are those striking NNE-SSW to NE-SW. These are the structures whose poles lie around the maximum principal stress (Figure 9).

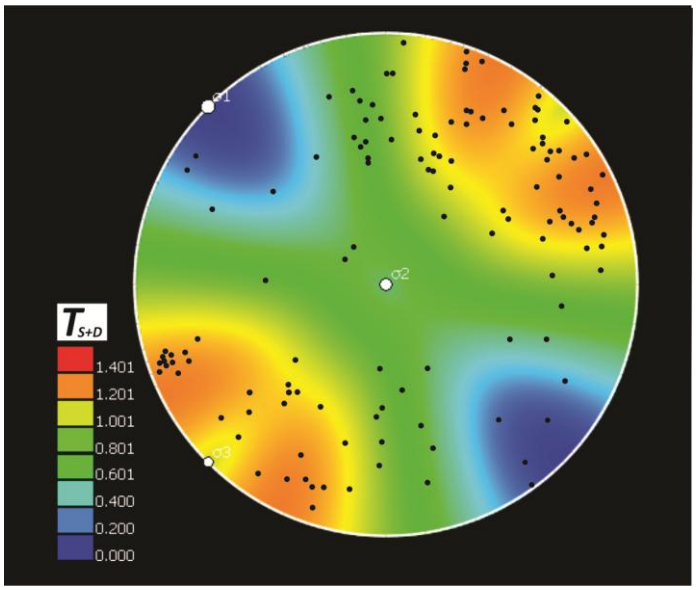

Figure 9. Stereonet of the combined slip and dilation tendencies. Fracture planes are represented as poles. Regions of higher slip and dilation tendencies are shown in warm colors whilst areas with the lowest tendencies are in cold colours. Present-day stress conditions are based on the orientations in Rangin *et al.* [34]. For complete results on the various scenarios, refer to Pastoriza [27]

Discussion

The fieldwork reveals the presence of two characteristically different groups of structures (Group 1 and 2) which accommodate three movement stages (Stages 1, 2a, and 2b) in the SNGF. These,

correspond to three brittle deformation events, with the most recent (Stage 2b) mostly being limited to reactivation of pre-existing structures rather than involving new fracture formation. Palaeostress inversion analysis suggests a transition between a strike-slip to an extensional to transtensional tectonic regime. Stage 1 likely occurred under a strike-slip to transpressive tectonic regime where S_{Hmax} is oriented NE-SW. This formed mainly WNW-ESE-trending sinistral faults and NE-SW tensile fractures. Based on the reported age of the Southern Negros Formation in which these fractures were observed exclusively, the Stage 1 fracturing event occurred no earlier than the Pliocene. The main sinistral faults run sub-parallel to the trace of the Puhagan Fault Zone which may suggest that it formed during Stage 1, but was initiated as a sinistral structure, contrary to its observed present-day kinematics.

The stress conditions then changed to a strongly extensional regime when most of the Group 2 fractures formed. New structures formed including WNW-ESE to NNW-SSE-trending normal, dextral, and oblique (normal/reverse) faults together with less common ENE-WSW-oriented normal faults. Associated NNW-SSE tensile fractures and smaller faults offset earlier Stage 1 fractures. The calculated principal extension direction is E-W for Stage 2a whilst principal compression is steep to vertical. Horizontal compression is probably minor given the nature of the suggested tectonic regime, but could conceivably be oriented N-S. There is a perceived counterclockwise rotation of the compression direction around the vertical from Stage 1 to Stage 2a, which may have persisted to the present-day, with a likely transitional phase captured by the Stage 2b deformation reactivating mainly pre-existing Group 2 fractures formed during Stage 2a. The overall tectonic setting during Stage 2b is also dominated by extension, with the principal extension direction, σ_3, now being NE-SW.

It is important to note here that the SNGF stress inversions have high misfit angles which imply that although the apparent *directions* of rotation are clear, the *amount* of rotation is rather less well

449 constrained. In the following sub-sections, we discuss geological processes that could potentially
450 explain the directions of the interpreted local stress rotations within SNGF.

451 The possibility of block rotations is partially constrained by a palaeomagnetic study by McCabe *et al.*
452 [39] that involved sampling and measurements at 86 sites across the Philippine Archipelago. Two
453 key rotation events were suggested. First, in the Early to Middle Miocene where it was suggested
454 that the islands of Panay, Cebu, and Mindanao rotated clockwise, whilst Marinduque rotated
455 counterclockwise. This, it was suggested, was related to the collision of the northern Palawan Block
456 with the Philippine Mobile Belt. Since Negros Island is bordered by Panay, Cebu, and Mindanao, it
457 may have also rotated clockwise at this time, but no Early to Middle Miocene samples were
458 collected from Negros to determine this. In the Late Miocene to Pliocene, McCabe *et al.* [39]
459 suggested that the central and northern parts of Luzon rotated clockwise potentially related to the
460 collision of the Luzon Arc with Taiwan. No rotation was observed in other parts of Philippines during
461 this period. Since then, it is suggested that the entire Philippine Arc has behaved as a single unit
462 with no discernible rotations based on the available palaeomagnetic data [39]. It is possible,
463 however, that the magnitude of any rotation that occurred close to the present-day may have been
464 too small for the study to capture.

465 Thus, these studies suggest that since the Pliocene, there is no strong palaeomagnetic evidence to
466 suggest that significant regional-scale block rotations have occurred in the island of Negros. This
467 seems consistent with the generally low displacements inferred along the major fault structures in
468 the SNGF, which suggests that the regional finite strain is low, meaning that significant fault-induced
469 block rotations related to these faults are unlikely. Thus it seems most likely that apparent changes
470 in stress orientations due to block rotation are unlikely to have occurred in the last 5 Myr since the
471 last plate reorganization happened [11, 40, 41]. Further, the direction of the observed rotations is
472 also not consistent even if a 'domino-style' rotation is considered (i.e. clockwise rotation of stress
473 axes due to the movement of two large sinistral faults). Therefore, it is most likely that the observed

474 stress rotations in the SNGF area are related to a smaller-scale heterogeneity in the regional stress
475 field. We now go on to consider two possible geological processes which might account for such a
476 locally controlled stress perturbation.

477 ***Possible influences of the Philippine Fault and propagation of the Yupisan Fault***

478 The observed stress rotation may reflect a smaller-scale disturbance that is related to the local
479 lateral propagation of displacement along the Yupisan Fault. The Yupisan Fault is a NNE-SSW
480 sinistral-reverse fault traversing the eastern coast of Negros in the north and passes through to the
481 west of the CDN volcano in the southern part of the island (Figure 1b; [26]). Stress rotation related
482 to the Yupisan Fault is explored by looking at the displacement vectors of the Yupisan Fault as it
483 continues to slip during the time of its formation (proposed to be during the Late Pliocene) and how
484 the displacement could affect the surrounding blocks, including the area where the CDN volcano is
485 located (details in Pastoriza [27]). Coulomb® 3.3 was used, which is a MatLab-based calculation and
486 visualisation program designed for the determination of static displacements, strains, and stresses at
487 any depth caused by a fault slip, magmatic intrusion, or dike expansion/contraction [42] following
488 the concepts in Toda *et al.* [43] and Lin and Stein [44].

489 For this analysis, the southern inland trace of the Yupisan Fault was divided into five segments based
490 on the curvature of the lineament observed on satellite imagery. The strike azimuth for each fault
491 segment was extracted from the digital elevation models whilst the dip angle is taken from the
492 earthquake focal mechanism data of the February 2012 Negros earthquake and was assumed to be
493 the same for all five segments. Using the USGS-calculated 6.7 earthquake magnitude along Yupisan
494 Fault in 2012, the amount of total co-seismic slip along the fault is estimated to be 0.524 m
495 (calculation after Wells and Coppersmith [45]). This net slip was then broken down into dip and
496 strike-slip components for each fault segment based on the estimated rake on that fault segment
497 using geometrical rules. The geometrical rake was approximated with the aid of stereographical
498 projections using the compression axis direction proposed by Rangin *et al.* [34].

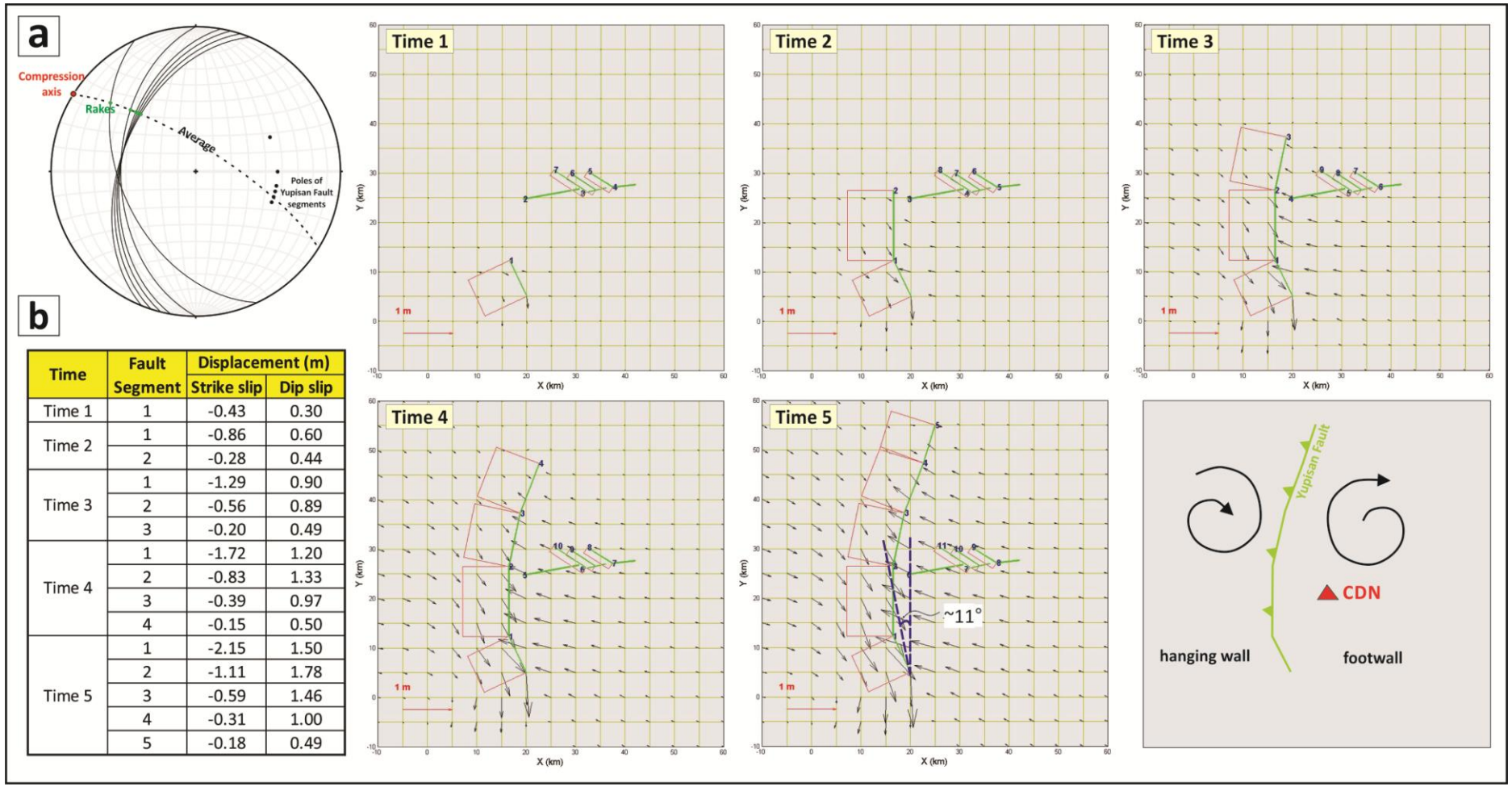

Time	Fault Segment	Displacement (m)	
		Strike slip	Dip slip
Time 1	1	-0.43	0.30
Time 2	1	-0.86	0.60
	2	-0.28	0.44
Time 3	1	-1.29	0.90
	2	-0.56	0.89
	3	-0.20	0.49
Time 4	1	-1.72	1.20
	2	-0.83	1.33
	3	-0.39	0.97
	4	-0.15	0.50
Time 5	1	-2.15	1.50
	2	-1.11	1.78
	3	-0.59	1.46
	4	-0.31	1.00
	5	-0.18	0.49

Figure 10. Displacement vector model of a northward propagating Yupisan Fault. Stereonet in the upper left shows the orientation of the Yupisan Fault segments discussed in-text. The table below it lists the amount of cumulative displacement per time for each fault segment, where a negative strike-slip displacement refers to sinistral movement along that fault segment. The boxes on the right show the propagation of Yupisan Fault from Time 1 to Time 5. Each fault segment is represented in green whilst the red boxes connected to it are the projected subsurface plane. Displacement vectors are shown as the black arrows. The green E-W and NW-SE lines at the centre of each box represent Puhagan Fault and some of the key structures within SNGF. Shown in the final box is the general rotation of the blocks for the footwall and hangingwall of the Yupisan Fault, where the CDN volcano and SNGF are on the footwall.

505 A propagating Yupisan Fault was then modelled using Coulomb® 3.3 for two scenarios – one where
506 the fault propagates northwards and another where it propagates southwards. The key assumption
507 here is that every time a new segment slips, the older segments slip with it. This basically confers a
508 cumulative displacement for each segment. Additionally, it is assumed that each time the Yupisan
509 Fault slips, an earthquake with the same magnitude of 6.7 is generated.

510 Figure 10 illustrates that the total amount of slip for each segment gradually increases as the Yupisan
511 Fault propagates. In a northward propagating model, at the first onset of the structure *Time 1*, the
512 southernmost segment slips 0.43 and 0.30 m along the strike and the dip, respectively (Figure 10).
513 By *Time 5,* it has slipped a total of 2.15 m sinistrally and 1.50 m along its dip. In a northward
514 propagating Yupisan Fault, this configuration induced a progressive clockwise block rotation on both
515 sides of the fault (Figure 10). The directions are the other way around for the stress rotations which
516 would be counterclockwise. These observations are opposite if a southward growing Yupisan Fault is
517 considered [27]. From Stage 2a to the present-day, an apparent counterclockwise rotation of the
518 stresses around the horizontal is observed (Figure 8). This observation therefore fits a northward
519 propagating Yupisan Fault model, where the footwall, in which the CDN and SNGF are situated,
520 appears to have rotated progressively clockwise, as the fault continued to move.

521 The model suggests that after five slip increments along the Yupisan Fault (*Time 5*), the southern
522 part of the footwall has rotated roughly 11° (Figure 10). This is close to the 9° rotation along the
523 horizontal from Stage 2b (144°) to the present-day (135° in [34]) (Figure 8) suggesting a potentially
524 good fit with the northward propagating Yupisan Fault as a potential trigger of the observed rotation
525 of the stresses within the SNGF. Further, considering that this modelling utilised the present-day
526 compression direction of 315°/135°, the consistency of the degree of rotation with the stress
527 inversion results suggest that the present-day stress conditions may have actually remained
528 relatively constant throughout Stage 2a and that the growing Yupisan Fault has triggered local block
529 rotations within its immediate vicinity resulting in an *apparent* rotation of the local stress fields.

Potentially, the observed change in tectonic regime between Stage 1 and Stage 2a could be due to changes in the stress magnitudes, leading to a 'flipping' of the stress axes, which does not necessarily require a drastic change in the far-field stress orientations. This illustrates how the growth of large-scale regional deformation structures may potentially affect smaller-scale stress fields.

Although we have initially eliminated the possibility of block rotation in Negros Island given that no palaeomagnetic data can support it, the smaller-scale rotation proposed herein is possible at low finite strains. A local palaeomagnetic study could help to test and refine this model, provided that a minimal rotation of 11° can be captured.

Changes in tectonic regime and the development of the CDN volcanic activity

Given the presence of an active subduction zone (Negros Trench) located to the southwest of the SNGF and a large reverse fault (Yupisan Fault) on its western flank (Figure 1a), a dominant horizontal compression direction might be expected for the study area. Although this is true for Stage 1, it does not seem to be the case during Stage 2a and Stage 2b which are both predominantly extensional based on the results of the palaeostress inversions and the observed dominance of normal faults.

The spatial and temporal effects of volcanism on the stress fields in the summit region of a volcano have been explored by a number of authors [e.g. 46, 47, 48]. Being centrally located in a volcanic complex, the potential influence of the CDN volcanic activity on the stress fields over time and the style of fracturing within the SNGF should not be disregarded. The CDN volcano is characterised by several episodes of volcanism and intrusion marked by thick sequences of volcanic deposits seen in the subsurface, with three distinct volcanic centers of varying ages exposed at the surface. Terakawa *et al.* [47] have shown that volcanic activity can induce temporal stress changes in the summit regions of erupting volcanoes. Thus, during the 2014 eruption of Mount Ontake in Japan, focal mechanisms indicate that normal-faulting dominated pre-eruption whilst reverse faulting

555 prevailed thereafter. Further, it was demonstrated that the average misfit angle of the focal
556 mechanisms around and in the periphery of the edifice significantly increased prior to the eruption.
557 An inflation under the volcano, which was driven by magmatic or hydrothermal fluids, was identified
558 as the cause of the stress perturbation, particularly resulting in the rotation of the maximum and
559 minimum principal stresses [47]. The results of this study and that of Vargas-Bracamontes and
560 Neuberg [49] amongst others, clearly illustrate how magma pressures can locally perturb and even
561 overpower the regional stress field in an area of active volcanism. This potentially results in local
562 stress fields being different from the prevailing large-scale conditions.

563 The dominance of mostly normal faults in the Group 2 fractures during both Stages 2a and 2b may
564 potentially be related to the inflation and gravity spreading of the CDN volcano and associated
565 intrusive emplacements. Formation of grabens along the flanks and *en echelon* strike-slip faults,
566 folds, and reverse structures at the base are typically observed on gravitational spreading volcanoes
567 based on analogue modelling [50] and field observations [51]. Similar structures are also observed
568 when the spreading is associated with magmatic intrusion. The abundance of extensional structures
569 in the SNGF may be associated with this type of spreading behaviour. With continued dyke
570 emplacements underneath the CDN, the volcano would continue to grow, requiring the surface to
571 expand. Such expansion is most easily accommodated by fracturing. This is consistent with the
572 observation that the southwest area of the geothermal field is most dissected by normal faults,
573 which is the closest to the main edifice (highest elevation mapped) and where the Nasuji Pluton is
574 laterally situated in the subsurface. Rae *et al.* [52] have illustrated that the intrusive events
575 underneath the CDN have influenced the alteration type and the propagation of heat below the
576 SNGF. It is perhaps not surprising then that during the several intrusion events, hydrofractures have
577 formed and are later reactivated as shear or as tensile structures.

578 Thus, volcanism, spreading, intrusion, and the geothermal processes, are likely to have
579 independently or altogether influenced the observed dominant normal-faulting regime within the
580 SNGF since Stage 2a.

581 **Synthesis and Conclusion**

582 Remote sensing studies and surface-based geological fieldwork conducted within the SNGF reveal
583 that the region is dominated by brittle deformation. Age indicators and cross-cutting relationships
584 suggest that at least two fracture-forming events occurred and have been locally reactivated under
585 evolving stress fields. The changes are most likely driven by regional and local tectonic, and volcanic
586 processes within Southern Negros. Although limited by the age of the oldest rocks exposed at the
587 surface, the deformation history proposed is constrained from the Middle Pliocene to the present
588 day. This assumes that the reported age of Late Pliocene to Early Pleistocene of the Southern
589 Negros Formation, which is purely based on field stratigraphic position is correct. A regional
590 structural evolution with time is illustrated in Figure 11a whilst a more detailed and localised view is
591 shown in Figure 11b.

592 By the Pliocene, the Philippine Fault had started to propagate in the eastern part of the Philippines
593 and the present-day plate vectors were already in-place. Southern Negros at this time was still
594 partly submerged underwater and the Southern Negros Formation, which formed as a result of the
595 volcanic activity of the palaeo-CDN, was deposited underwater in Puhagan (central part of the field)
596 but subaerially in the west [28]. An emergent volcanic edifice in the western part of the present-day
597 CDN may have existed at this time (Figure 11a.i). An early phase of brittle deformation, Stage 1,
598 occurred, affecting the SNF and, presumably, older lithologies. Stress inversion analyses of the
599 rather limited field data suggest a NE-SW-oriented horizontal maximum compression under a strike-
600 slip or transpressional regime, which is also consistent with the equivalent-age structures observed
601 in the country rocks to the northwest of SNGF in the Pamplona-Sta.Catalina area [27]. In southern
602 Negros, a sinistral ENE-WSW-trending *en echelon* palaeo-Puhagan Fault is thought to have been

603 present, running across the northern flanks of the palaeo-CDN edifice (Figure 11b). Associated with
604 this major structure were a series of E-W sinistral faults and NE-SW tensile fractures cutting the early
605 SNF and older rocks (Figure 11b). During this time, a smaller hydrothermal system may have existed
606 which may be related to early intrusions (e.g. Puhagan dykes in [28]). The SNF rocks experienced
607 intense preliminary alteration whilst fractures were channeling sulphide-rich fluids. A dominantly
608 reducing environment, maybe because of less interaction with surface waters prevailed, meaning
609 that these fluids deposited widespread pyrite along the fractures. Cockade structures within the
610 pyrite veins suggest episodic influxes of sulphide-rich fluids into open fracture systems over
611 significant timescales [30].

612 By the end of the Pliocene, it is suggested that the Yupisan Fault had started to propagate
613 northwards from the SSW coast of Southern Negros towards the eastern coast of the island, under a
614 stress regime similar to the present day, i.e. NW-SE horizontal compression ([34]; Figure 11a.ii). The
615 palaeo-CDN continued its activity and deposition of SNF was maintained. In the Early to Middle
616 Pleistocene, emplacement of the main Nasuji Pluton [18] and associated intrusions occurred,
617 particularly in the western part of the SNGF. This intrusion triggered significant steam-heated argillic
618 alteration in the western area of the geothermal field which is one of the earliest dated
619 hydrothermal alteration episodes (0.7 Mya in Rae *et al.* [52] and 0.81 Mya in Takashima and Reyes
620 [53]) in the SNGF. Leach and Bogie [54] concluded that this process may have introduced a barren
621 porphyry-copper type deposit, which they considered to be the relict alteration suite observed in the
622 SNGF boreholes today. An overpressured magma chamber resulting from the intrusion may have
623 induced hydrofracturing in the immediate vicinity of the pluton. This drastically increased the
624 degree of fracturing in the western sector, which is exhumed today.

625

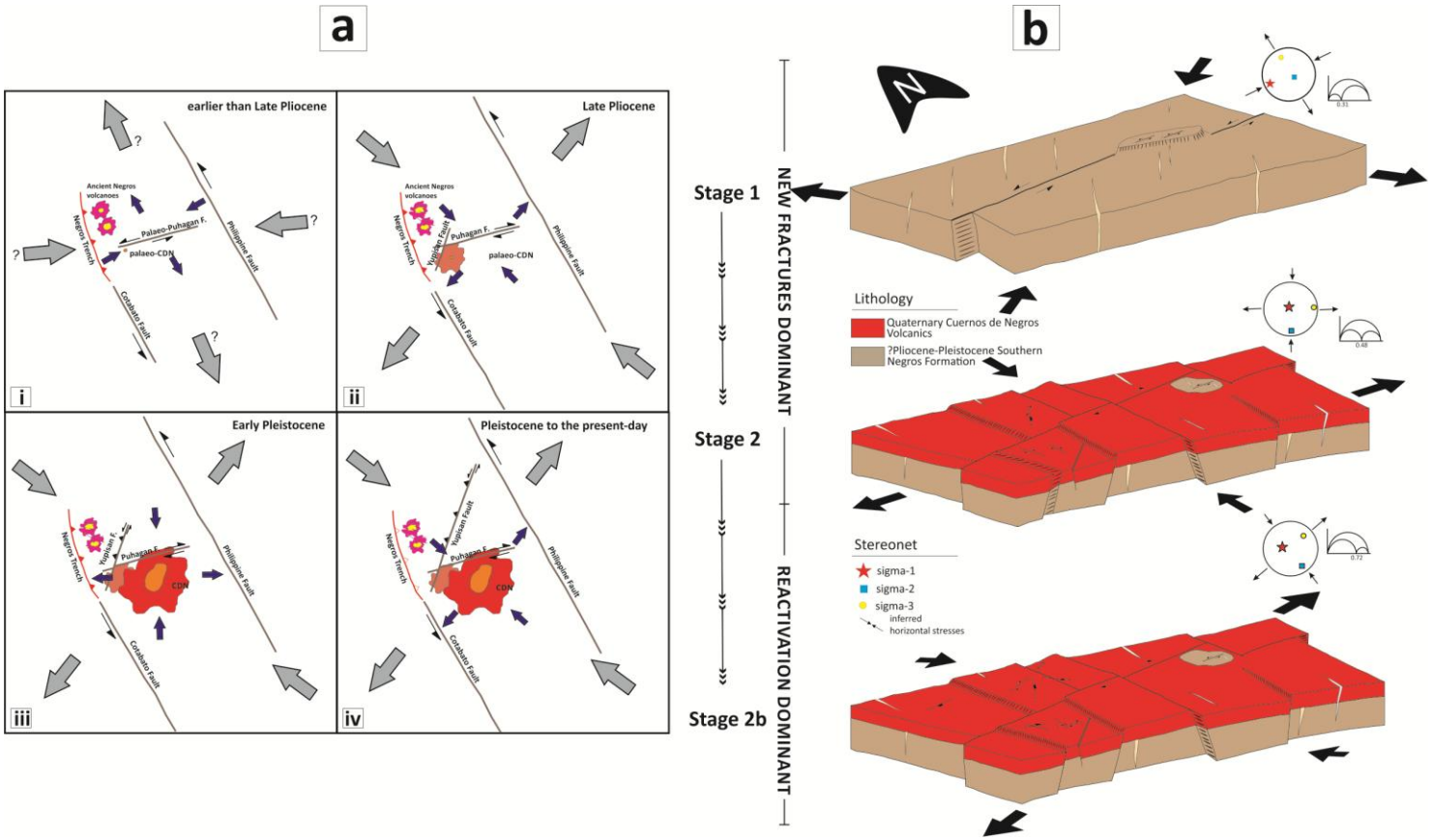

626

627 **Figure 11. Structural evolution of the Southern Negros and the SNGF**. (a) Simplified diagram of the tectonic evolution of the Cuernos de Negros volcanic complex and its relationship with
628 the key regional structures in the Philippines (i.e. Philippine and Cotabato Faults). (i) to (iv) represent a progressive evolution with increasing time. (b) For SNGF, the model focuses on the
629 three stages of fracturing. Apparent changes in stress directions suggested in the palaeostress inversion which could be a function of small-scale block rotation are indicated. Note that the
630 sketches are not drawn to scale. The stereonets and the Mohr circles are generated in MyFault. Stage 1 at the local scale is contemporaneous with (i) at the regional scale, whilst Stages 2a
631 and 2b occurred during (iii) and (iv) at the regional scale, respectively.

The Pleistocene marked the peak of the volcanic activity of the CDN complex which led to the deposition of lava flows and pyroclastics. It is suggested that a regional NW-SE compressional stress regime dominated in the SNGF and reactivated the palaeo-Puhagan Fault with dextral-strike slip kinematics (Figure 11a/b). Its kinematics is clearly observed today based on the modern geomorphology, offsetting the CDN complex and the Yupisan Fault right-laterally. This formed NW-SE dextral Riedel structures related to the Puhagan Fault in the northern part of SNGF. Locally, with a more active volcano formation, a localised extensional setting prevailed under Stage 2a, with the dominant extension somewhat consistent with the regional extension direction (Figure 11a.iii), where WNW-ESE to NNW-SSE normal, dextral, and oblique (normal/reverse) and rare ENE-WSW normal faults propagated. NNW-SSE-trending tensile fractures clearly offset the earlier tensile and sinistral structures. In the northern area of the field, the earlier hydrofractures were reactivated as shear fractures. The heat in the subsurface particularly shifted towards the central part of the SNGF (central Okoy) following the conduction-convection model of Takashima and Reyes [53]. With the now crystallised dykes and/or pluton, Rae *et al.* [52] suggested that the circulation became more diluted, being affected by meteoric water, and less influenced by hydrothermal sources. This led to a propylitic and illite-rich alteration, affecting the immediate country rock. Consequently, Stage 2a fractures are in most cases host to thick clay alteration and iron-oxide formation.

During the Holocene, the volcanic activity in the CDN waned, thus the regional stress fields became more prevalent within the SNGF, but still under a local extensional/transtensional setting (Figure 11a.iv and Figure 11b). The final fracturing transpired during Stage 2b formed mostly NW-SE-oriented normal faults. Reactivation of the Stage 2a fractures, mostly as dip-slip structures was also common. By this time, the heat was now centered in Puhagan as a result of either shifting due to convection-conduction [53] or because a younger intrusion event occurred underneath the area as proposed by Rae *et al.* [18]. Many of these young structures served as channels in the present-day hydrothermal system towards the surface, appearing as a result of the concentration of active

thermal manifestations around Puhagan today. This suggests that a majority have remained open and active in the present-day stress configuration.

The results of the slip and dilation tendency analysis suggesting that NW-SE-oriented fractures should in theory be the best and most permeable drilling targets. This agrees with actual drilling results in SNGF [55]. However, the slip and dilation tendencies indicate that NE-SW and NNE-SSW-oriented structures should be the least permeable as they are likely presently stable; they are, however, also known to be important in the fluid flow regime of the SNGF based on actual boreholes [55]. These large-scale NE-SW faults could have been original tensile fractures formed during Stage 1 and could have been reactivated during succeeding fracturing events. Such reactivation may have re-opened these structures at depth as tensile fractures in the predominantly extensional regime of Stage 2a +/- a component of shearing. As the geothermal system was already developing during Stages 2a and 2b, temperatures at the fracturing depths may well have been much higher, making rapid cementation/sealing of the fracture planes less likely. This reactivation model may explain why some larger NE-SW faults have remained opened until the present day and consequently, are proven to be permeable channels of geothermal fluids in the SNGF [55].

This work is by far the most comprehensive geological analysis and the first microtectonic work on the SNGF surface geological data. Several structural field campaigns and studies have been done in the field over the last 30 years [56-62] as part of its exploration and development works. However, geological interpretations were limitedly based on orientation analysis (i.e. the orientation of the fractures with the highest frequency correlated to the orientation of the regional structure) with very minimal attempts to rank or prioritize structures with varying characteristics. There was a significant lack of the appreciation of the kinematics of mapped faults and their implication to potential subsurface permeability, and consequently the drilling strategy.

The work presented here addresses that gap by illustrating a more comprehensive approach to surface geological data analysis. From a thorough characterization of the mapped faults (e.g.

682 fracture fills, kinematics), their cross-cutting relationships, and a stress inversion, one can build the
683 deformation history of the field. With a refined geological history and the information on the
684 associated fluid alteration for each phase, a better understanding on which structures related to the
685 geothermal development can be provided. Further, the utilization of the slip and dilation tendency
686 analysis is a useful tool in the identification of the potential interaction of the mapped faults with the
687 present-day stresses, and how this may influence fluid flow. This could help to delineate structures
688 which are currently stressed, and thus may be potential drilling targets given the likely increased
689 fracture intensity and widening of the fracture aperture.

690 This work illustrates how a strongly field-based geological approach can inform exploration and
691 eventual development strategies for drilling, even at the early stages of the field exploration (i.e.
692 even prior to drilling), and can be further enhanced by incorporating a multi-scale fracture attribute
693 and topology analysis as presented in Pastoriza [27]. This geological workflow should supplement
694 existing workflows for building conceptual models at the exploration stage (e.g. Cumming [63]) and
695 when integrated with geochemical, geophysical, and hydrological data, be usefully employed for
696 field-scale development of geothermal resources.

697 **Funding statement**

698 This work is part of the PhD thesis of the main author at Durham University, generously funded by
699 the Energy Development Corporation.

700 **Data Availability**

701 The data that support the findings of this study are available from the Durham University E-Theses
702 Repository, but restrictions apply to the availability of these data, under a confidentiality agreement
703 between the Energy Development Corporation and Durham University. Data are however available
704 from the authors upon reasonable request and with permission to the Energy Development
705 Corporation.

Conflicts of interest

The authors declare that there is no conflict of interest regarding the publication of this paper. Energy Development Corporation has reviewed and granted permission to publish this work.

Acknowledgements

Due acknowledgment to the Energy Development Corporation for granting access to internal reports and well data. To Jonathan Kit Reyes and Ferdie Castillejo for the assistance in the field campaigns in Negros. To Mario Aurelio, Jon Gluyas, and Richard Walker for their contributions in the entire project. To Nick Primaleon and the two anonymous reviewers for their constructive criticisms to improve this paper.

References

1. Huenges, E., ed. *Geothermal energy systems*. 2010, Wiley-VCH: Weinheim, Germany.
2. Ochieng, L. *Overview of geothermal surface exploration methods*. in *Short Course VIII on Exploration for Geothermal Resources*. 2013. Kenya.
3. Dobson, P.F., et al., *Porosity, permeability, and fluid flow in the Yellowstone geothermal system, Wyoming.* Journal of Volcanology and Geothermal Research, 2003. **123**(3–4): p. 313-324.
4. Schutter, S.R., *Hydrocarbon occurrence and exploration in and around igneous rocks.* Geological Society, London, Special Publications, 2003. **214**(1): p. 7-33.
5. Coppo, N., et al. *3-D magnetotelluric investigations for geothermal exploration in Martinique (Lesser Antilles). Characteristic deep resistivity structures, and shallow resistivity distribution matchin heliborne TEM results*. in *Proceedings World Geothermal Congress* 2015. Melbourne, Australia.
6. Ciriaco, A.E. and M. O'Sullivan. *3D dual porosity modeling of tracer transport in Palinpinon 1 Geothermal Field, Philippines*. in *World Geothermal Congress*. 2015. Melbourne, Australia.
7. Magro, G., F. Gherardi, and F.E.B. Bayon, *Noble and reactive gases of Palinpinon geothermal field (Philippines): Origin, reservoir processes and geodynamic implications.* Chemical Geology, 2013. **339**: p. 4-15.
8. Cardwell, R.K., B.L. Isacks, and D.E. Karig, *The spatial distribution of earthquakes, focal mechanism solutions, and subducted lithosphere in the Philippine and Northeastern Indonesian Islands*, in *The tectonic and geologic evolution of Southeast Asian seas and islands*, D.E. Hayes, Editor 1980, American Geophysical Union. p. 1-35.
9. Yumul, G.P., C.B. Dimalanta, and R.A. Tamayo, *Indenter-tectonics in the Philippines: Example from the Palawan Microcontinental Block - Philippine Mobile Belt Collision.* Resource Geology, 2005. **55**(3): p. 189-198.

10. Gervasio, F.C., *The age and nature of orogenesis in the Philippines.* The Philippine Geologist, 1966. **20**(4): p. 121-140.
11. Mines and Geosciences Bureau, *Geology of the Philippines*, M.A. Aurelio and R.E. Pena, Editors. 2010: Quezon City.
12. Sarewitz, D.R. and D.E. Karig, *Geologic evolution of Western Mindoro Island and the Mindoro Suture Zone, Philippines.* Journal of Southeast Asian Earth Sciences, 1986. **1**(2): p. 117-141.
13. Aurelio, M.A., *Shear partitioning in the Philippines: constraints from Philippine fault and global positioning system data.* The Island Arc, 2000. **9**: p. 584-597.
14. DeMets, C., R.G. Gordon, and D.F. Argus, *Geologically current plate motions.* Geophysical Journal International, 2010. **181**(1): p. 1-80.
15. Heidbach, O., et al., *Plate boundary forces are not enough: Second- and third-order stress patterns highlighted in the World Stress Map database.* Tectonics, 2007. **26**(6): p. n/a-n/a.
16. Lagmay, A.M.F., A.M.P. Tengonciang, and H.S. Uy, *Structural setting of the Bicol Basin and kinematic analysis of fractures on Mayon Volcano, Philippines.* Journal of Volcanology and Geothermal Research, 2005. **144**(1–4): p. 23-36.
17. Yu, S.-B., et al., *Present-day crustal deformation along the Philippine Fault in Luzon, Philippines.* Journal of Asian Earth Sciences, 2013. **65**(0): p. 64-74.
18. Rae, A.J., et al., *The nature of magmatism at Palinpinon geothermal field, Negros Island, Philippines: implications for geothermal activity and regional tectonics.* Journal of Volcanology and Geothermal Research, 2004. **129**(4): p. 321-342.
19. Jarvis, A., et al., *Hole-filled SRTM for globe Version 4, available from the CGIAR-CSI SRTM 90m Database*, 2008.
20. Barrier, E., P. Huchon, and M. Aurelio, *Philippine fault: A key for Philippine kinematics.* Geology, 1991. **19**(1): p. 32-35.
21. Solidum, R.U., P.R. Castillo, and J.W. Hawkins, *Geochemistry of lavas from Negros Arc, west central Philippines: Insights into the contribution from the subducting slab.* Geochemistry, Geophysics, Geosystems, 2003. **4**(10): p. 9008.
22. Garwin, S., R. Hall, and Y. Watanabe, *Tectonic setting, geology, and gold and copper mineralization in Cenozoic magmatic arcs of Southeast Asia and the West Pacific Appendix 1.* Society of Economic Geologists, Inc. Economic Geology, 2005. **100**: p. 891-930.
23. Biedersee, H.v. and H. Pichler, *The Canlaon and its neighbouring volcanoes in the Negros Belt, Philippines.* Journal of Southeast Asian Earth Sciences, 1995. **II**(2): p. 111-123.
24. GVP. *Kanlaon: eruptive history*. 2018; Available from: http://www.volcano.si.edu/volcano.cfm?vn=272020#bgvn_3202.
25. Rangin, C., C. Muller, and H. Porth, *Neogene geodynamic evolution of the Visayan Region*, in *On the geology and hydrocarbon prospects of the Visayan Basin, Philippines*, H. Porth and C.H. Von Daniels, Editors. 1989, Geologisches Jahrbuch. p. 7-28.
26. Aurelio, M.A., et al., *Seismotectonics of the 6 February 2012 Mw 6.7 Negros Earthquake, central Philippines.* Journal of Asian Earth Sciences, 2017. **142**: p. 93-108.

27. Pastoriza, L.R., *The geological characterisation and permeability evaluation of fractures in the Southern Negros Geothermal Field, Negros Island, Philippines*, in *Earth Sciences*2017, University of Durham.
28. Ariceto-Villarosa, H.G., et al., *The subsurface geology and alteration mineralogy of Nasuji-Sogongon Sector, Southern Negros Geothermal Field*, 1988, PNOC-Energy Development Corporation Internal Report.
29. Zaide, M., *Interpretation of rock-dating results in the Southern Negros Geothermal Field*, 1984, PNOC-EDC Internal Report.
30. Frenzel, M. and N.H. Woodcock, *Cockade breccia: Product of mineralisation along dilational faults.* Journal of Structural Geology, 2014. **68, Part A**: p. 194-206.
31. Michael, A.J., *Use of focal mechanisms to determine stress: A control study.* Journal of Geophysical Research: Solid Earth, 1987. **92**(B1): p. 357-368.
32. Michael, A.J., *Determination of stress from slip data: Faults and folds.* Journal of Geophysical Research: Solid Earth, 1984. **89**(B13): p. 11517-11526.
33. Dichiarante, A.M., *A reappraisal and 3D characterisation of fracture systems within the Devonian Orcadian Basin and its underlying basement: an onshore analogue for the Clair Group*, in *Earth Sciences*2017, University of Durham: Durham.
34. Rangin, C., et al., *Plate convergence measured by GPS across the Sundaland/Philippine Sea Plate deformed boundary: the Philippines and eastern Indonesia.* Geophysical Journal International, 1999. **139**(2): p. 296-316.
35. Kreemer, C., et al., *Active deformation in eastern Indonesia and the Philippines from GPS and seismicity data.* Journal of Geophysical Research: Solid Earth, 2000. **105**(B1): p. 663-680.
36. Ferrill, D.A., et al., *Stressed rock strains groundwater at Yucca Mountain, Nevada.* GSA Today, 1999. **9**(5): p. 2-7.
37. Moeck, I., G. Kwiatek, and G. Zimmermann, *Slip tendency analysis, fault reactivation potential and induced seismicity in a deep geothermal reservoir.* Journal of Structural Geology, 2009. **31**(10): p. 1174-1182.
38. Rangin, C., *Rigid and non-rigid micro-plates: Philippines and Myanmar-Andaman case studies.* Comptes Rendus Geoscience, 2016. **348**(1): p. 33-41.
39. McCabe, R., et al., *Paleomagnetic results from Luzon and the central Philippines.* Journal of Geophysical Research: Solid Earth, 1987. **92**(B1): p. 555-580.
40. Aurelio, M., *Tectonics of the Philippines revisited.* Journal of the Geological Society of the Philippines, 2000. **55**(3/4): p. 119-183.
41. Aurelio, M.A., R.E. Peña, and K.J.L. Taguibao, *Sculpting the Philippine archipelago since the Cretaceous through rifting, oceanic spreading, subduction, obduction, collision and strike-slip faulting: Contribution to IGMA5000.* Journal of Asian Earth Sciences, 2013. **72**: p. 102-107.
42. Toda, S., et al., *Coulomb 3.3. graphic-rich deformation and stress-change software for earthquake, tectonics, and volcano reserach and teaching - user guide*, 2011, U.S. Geological Survey Open-File Report 2011-1060: Reston, Virginia.
43. Toda, S., et al., *Forecasting the evolution of seismicity in southern California: Animations built on earthquake stress transfer.* Journal of Geophysical Research: Solid Earth, 2005. **110**(B5).
44. Lin, J. and R.S. Stein, *Stress triggering in thrust and subduction earthquakes and stress interaction between the southern San Andreas and nearby thrust and strike-slip faults.* Journal of Geophysical Research: Solid Earth, 2004. **109**(B2).

45. Wells, D.L. and K.J. Coppersmith, *New empirical relationships among magnitude, rupture length, rupture width, rupture area, and surface displacement.* Bulletin of the Seismological Society of America, 1994. **84**(4): p. 974-1002,A1-A4,B1-B11,C1-C49.
46. Roman, D.C., et al., *Temporal and spatial variation of local stress fields before and after the 1992 eruptions of Crater Peak vent, Mount Spurr volcano, Alaska.* Bulletin of the Seismological Society of America, 2004. **94**(6): p. 2366-2379.
47. Terakawa, T., et al., *Monitoring eruption activity using temporal stress changes at Mount Ontake volcano.* Nat Commun, 2016. **7**.
48. Sánchez, J.J., M. Wyss, and S. R. McNutt, *Temporal-spatial variations of stress at Redoubt volcano, Alaska, inferred from inversion of fault plane solutions.* Journal of Volcanology and Geothermal Research, 2004. **130**(1–2): p. 1-30.
49. Vargas-Bracamontes, D.M. and J.W. Neuberg, *Interaction between regional and magma-induced stresses and their impact on volcano-tectonic seismicity.* Journal of Volcanology and Geothermal Research, 2012. **243–244**: p. 91-96.
50. Delcamp, A., et al., *Relationships between volcano gravitational spreading and magma intrusion.* Bulletin of Volcanology, 2012. **74**(3): p. 743-765.
51. Borgia, A. and B. van Wyk de Vries, *The volcano-tectonic evolution of Concepción, Nicaragua.* Bulletin of Volcanology, 2003. **65**(4): p. 248-266.
52. Rae, A.J., et al., *Spatial and temporal relationships between hydrothermal alteration assemblages at the Palinpinon geothermal field, Philippines: implications for porphyry and epithermal ore deposits.* Society of Economic Geologists, Special Publication, 2003. **10**: p. 223-246.
53. Takashima, I. and A.G. Reyes, *Alteration and TL age of the Palinpinon geothermal area, Negros Island, southern Philippines.* JGRSJ, 1990. **12**(4): p. 315-325.
54. Leach, T.M. and I. Bogie. *Overprinting of hydrothermal regimes in the Palinpinon geothermal field, Southern Negros, Philippines*. in *4th New Zealand Geothermal Workshop*. 1982. Auckland, New Zealand.
55. Bayon, F.E.B. and M.S. Ogena. *Handling the problem of rapid reinjection returns in Palinpinon-I and Tongonan, Philippines*. in *World Geothermal Congress*. 2005. Antalya, Turkey.
56. Pornuevo, J.B. and R.O. Obusan, *Structural mapping at Nasuji-Sogongon and Puhagan Sectors, Southern Negros Geothermal Field, Negros Oriental*, 1983, PNOC-EDC Internal Report.
57. Tebar, H.J., *Structural mapping at West Nasuji-Sogongon Sector, Southern Negros Geothermal Field, Negros Oriental*, 1984, PNOC-EDC Internal Report.
58. Batolbatol, J.R. and M.R.D. Fermin, *Surface structures of Nasuji-Sogongon Sector, Southern Negros Geothermal Field*, 2014, Energy Development Corporation Internal Report.
59. Salonga, N.D., *Surface structures of Okoy Sector, Southern Negros Geothermal Field*, 1989, PNOC-EDC Internal Report.
60. Cerio, M. and F. Tosco, *Dauin Geothermal Prospect - Geology*, 2014, Energy Development Corporation Internal Report.
61. Alincastre, R.S., *Geology of Baslay-Dauin prospect*, 1982, PNOC-EDC Internal Report.
62. Tebar, H.J., D.Z. Hermoso, and R.G. Lapuz, *Geology of North Okoy geothermal prosposect, Southern Negros Geothermal Field, Negros Oriental*, 1984, PNOC-Energy Development Corporation Internal Report.

63. Cumming, W. *Geothermal resource conceptual models using exploration data*. in *Thirty-Fourth Workshop on Geothermal Reservoir Engineering* 2009. Stanford, California.